UNIVERSITY OF OKLAHOMA

GRADUATE COLLEGE

MERAMEC VELOCITY SYSTEMATICS

A THESIS

SUBMITTED TO THE GRADUATE FACULTY

in partial fulfillment of the requirements for the

Degree of

MASTER OF SCIENCE

By

JING FU
Norman, Oklahoma
2020

MERAMEC VELOCITY SYSTEMATICS

A THESIS APPROVED FOR THE
MEWBOURNE SCHOOL OF PETROLEUM AND GEOLOGICAL ENGINEERING

BY THE COMMITTEE CONSISTING OF

Dr. Carl H. Sondergeld, Chair

Dr. Chandra S. Rai

Dr. Deepak Devegowda

To my professors, family, and friends.

ACKNOWLEDGEMENTS

This research was funded through Marathon Oil Corporation. I thank the Marathon Oil Company and the Oklahoma Petroleum Information Center (OPIC) for laying out and granting access to Meramec cores for measurement. The encouragement of Chris McLain from Marathon Oil Corporation is greatly appreciated.

I am indebted to my advisors, Dr. Carl Sondergeld and Dr. Chandra Rai, for providing me with the opportunity to be part of their Integrated Core Characterization Center (IC^3) research group and their mentorship, support, patience, and knowledge throughout the extent of the project. I would like to thank Dr. Deepak Devegowda for his input and support. I am thankful to Dr. Tinni, Dr. Curtis, Bruce Spears, Gary Stowe, Micaela Langevin, and Jeremy Jernigen for their help during the various stages of this research work.

I appreciate IC^3 graduate students, especially Son Dang, for sharing their insights and undergraduate students for their assistance. I would also like to thank my friends Byeungju, Heyleem, Son, Juan, Sanchay, Sidi, Pritesh for making my life at OU, a memorable one.

I express my sincere gratitude to my parents for their love, patience, and support.

TABLE OF CONTENTS

TABLE OF CONTENTS vi
1 INTRODUCTION 1
1.1 Synopsis 4
2 LITERATURE REVIEW 6
2.1 Wave propagation 6
2.2 Anisotropy 8
2.3 Parameters that affect velocities: 12
2.3.1 Porosity 12
2.3.1 Mineralogy 14
2.3.2 Effect of pressure and temperature 17
2.4 Vp-Vs relation 19
3 GEOLOGICAL SETTING 22
4 EXPERIMENTAL METHODOLOGY 25
4.1 Porosity measurements 25
4.2 Mineralogy measurements: FTIR and XRF 26
4.3 Ultrasonic measurements 27
5 RESULTS AND DISCUSSION 29
5.1 Sample description 29
5.2 Anisotropy 30
5.3 Porosity 33
5.4 Mineralogy 33
5.5 Velocity – porosity, mineralogy relationship 35
5.6 Pressure dependence 36
5.7 Velocity systematics (Wells) 38
5.7.1 Method 1 38
5.7.2 Method 2 39
5.7.3 Validation 41
5.8 Velocity systematics (Zonation) 46
6 CONCLUSION 51
7 REFERENCES 53

LIST OF TABLES

Table 2-2 Linear Regressions Vs-Vp (km/s) for Sandstone and Shale (Brine-Saturated) 19
Table 5-1 Summary of sample numbers 30
Table 5-2 Vp-Vs equations of all layers (velocities in km/sec) 49
Table 5-3 Vp-Vs equations of grouped Meramec layers (velocities in km/sec) 50

LIST OF FIGURES

Figure 2.1 P-wave and S-wave propagation (NDT Resource Center, 2017). 7

Figure 1.1 Schematic showing P-wave and polarized S-wave propagation through a laminated medium (Lo et al., 1986). 7

Figure 2.3 Transmitter and receiver are rotated simultaneously through an azimuth aperture of 180°. When particle motion is either parallel or perpendicular to the shale fabric, only one arrival wave is seen. At other angles, both slow and fast waves are present (Sondergeld and Rai, 1992). 8

Figure 3.1. Geological provinces of Oklahoma. Study area is highlighted in orange. The Sooner trend is located on the northeastern shelf of the Anadarko Basin (modified from Northcutt and Campbell, 1996). 22

Figure 3.2 Mississippian stratigraphic column is displayed next to the sea level cyclicity of the Carboniferous and Permian periods. The Meramec is deposited during increasing cyclicity due in part to the climatic transition of the Mississippian, resulting in complex stacking patterns and lateral distribution of facies. (Modified from Boyd, 2008; Haq and Schutter, 2008; Miller, 2019; Hardisty, 2019). 23

Figure 4.1 Chart showing all the lab measurements that were done on the samples used in this study. 25

Figure 4.2 Velocity measurement setup. The sample is placed between two endcaps and wrapped with a rubber boot. The rubber boot provides a seal between sample and pressurizing oil. Uniform confining pressure is provided by oil. Computer controlled switching allows sequential activation of the P-wave and two polarized shear wave transducers. 28

Figure 4.3 Example of the picked arrival time of P-wave. Waveforms are acquired at each confining pressure step. The first arrival time is shown as a pink line. 28

Figure 5.1 Map of wells in the study area. Seven wells are included in this study and the depositional trend of the study area is NW-SE. Wells are named following the depositional trend. 29

Figure 5.2 Velocity measured from different orientations. Vp_horiozntal, Vs_fast, and Vs_slow can be measured from horizontal plugs. Vp_vertical and Vs_slow can be measured from vertical plugs. Bedding planes are shown as grey lines. Propagation directions are red arrows, while the green and blue arrows indicate shear wave polarization directions. 31

Figure 5.3 Thomsen's anisotropy parameters of all samples. Number of samples for each well are shown in the brackets. More than 90% of samples have anisotropy parameters of less than 0.1. 32

Figure 5.4 SEM images of samples from layer 2,3,4, and 5. All scale bars are same (50 μm). Significant variation in rock microstructure observed throughout the well. Variations in grain size as well as dominant

mineralogy is observed. No strong preference for orientation of grains which matches with the low anisotropy calculated from velocity measurement. 32

Figure 5.5 Total porosity of samples from different wells. The total number of samples from each well are shown in the brackets. The well order follows the depositional trend. Different wells are shown in different colors. 33

Figure 5.6 Mineralogy measured using transmission FTIR. Wells are in the order of depositional trend (NW-SE). Different minerals are shown in different colors. The higher frequency displayed in well 4 is simply a consequence of finer sampling. 34

Figure 5.7 XRF-FTIR mineralogy comparison. The x-axis is FTIR mineralogy in weight percentage and the y-axis is XRF mineralogy inverted from XRF elements in weight percentage. They show a reasonable match. 34

Figure 5.8 Mineralogy measured using XRF. Wells are in the order of the depositional trend (NW-SE). Different minerals and Meramec zonation are shown in different colors. Following the depositional trend, the clay content is increasing. 35

Figure 5.9 Scatter plots of porosity, mineralogy and velocity. Vp and Vs show a clear linear trend. Both Vp and Vs decrease with increasing porosity and clays content. There is no clear correlation between quartz, feldspar, and velocity. 36

Figure 5.10 Acoustic velocities of all horizontal samples as a function of effective pressure. Effective pressure is from 500 psi to 4000 psi. 37

Figure 5.11 Acoustic velocities of all vertical samples as a function of effective pressure. Effective pressure is from 500 psi to 4000 psi. 37

Figure 5.12 Shear wave anisotropy of all horizontal samples. More than 90% of samples have an anisotropy parameter, γ, of less than 0.1. 38

Figure 5.13 Measured velocities on all vertical and low horizontal samples from all wells. The measured velocities from different wells are shown in different colors. The correlation between Vp-Vs is shown as a black line. 39

Figure 5.14 Correlation between gamma and epsilon (Sondergeld and Rai, 2011). 40

Figure 5.15 Measured vertical and converted horizontal sample velocities of all wells. The velocities of different wells are shown in different colors. The correlation of Vp-Vs is shown as a black line. 40

Figure 5.16 Vs residuals using the Vp-Vs equation. a) Vs residuals calculated using the equation created from the first method. The residuals range between -0.4 to 0.4; b) Vs residuals calculated using the equation created from the second method. The residual range between -0.6 to 0.6. 41

Figure 5.17 Test well locations are shown on the map. The first test well is 10 miles away from Well 4 and the second test well is 10 miles away from Well 7. 42

Figure 5.18 a) The Vp and Vs from wireline measurement, and predicted Vs using the Meramec velocity systematic of first test well. b) The Vp and Vs from wireline measurement, and predicted Vs using the Meramec velocity systematic of first test well. The measured Vs and predicted Vs of both test wells show good agreement. 43

Figure 5.19 The Vs residual, GR log, Vsh estimated from GR log, and the caliper log for Test 1 well are shown as black, orange, blue and green, respectively. The velocity comparison between log and systematic is in the last track. The Vs estimation error is less than 6%. 44

Figure 5.20 The Vs residual, GR log, Vsh estimated from GR log, and caliper log of Test 2 well are shown as black, orange, blue and green, respectively. The velocity comparison between log and systematic is in the last track. Zones has large estimation error are shown in the blue box. There is a positive correlation between washouts and Vs residual. 45

Figure 5.21 Comparison of Meramec formation systematic with reported unconventional Vp-Vs velocity systematics (Vernik, 2018), including the Castagna mudrock systematic. 46

Figure 5.22 Leco-TOC measured from Well 2, 3, 6, and 7. Sample number are labeled following well names. It shows that the formation contains little to no organics (less than 5%). 46

Figure 5.23. Mississippian stratigraphic column is displayed next to the sea level cyclicity of the Carboniferous and Permian periods. The Meramec is deposited during increasing cyclicity due in part to the climatic transition of the Mississippian, resulting in intricate stacking patterns and lateral distribution of facies. (Modified from Boyd, 2008; Haq and Schutter, 2008; Miller, 2019; Hardisty, 2019). 47

Figure 5.24 Measured vertical and low gamma horizontal sample velocities of Meramec zones. The velocities of different zones are shown in different colors. The correlations of Vp-Vs are shown as dash lines. 48

Figure 5.25 Measured vertical and low gamma horizontal sample velocities of grouped Meramec zones. The velocities of different groups are shown in different colors. The correlations of Vp-Vs are shown as solid lines. 49

ABSTRACT

Elastic wave velocities are often used to interpret formation properties, such as porosity, mineralogy, and lithology. Shear wave velocity systematics are valuable in creating elastic models when only P-wave sonics exists in legacy wells. Although considerable research has been carried out on conventional reservoir velocity systematics, the systematics for unconventional formations remain ill defined. In this study, a Vs-Vp systematic is developed for the Meramec formation, using laboratory pulse transmission ultrasonic measurements. The influences of porosity and mineralogy on velocities are discussed and a comparison between Meramec velocity systematic and existing literature systematics is provided.

The Vp and Vs measurements on 385 dodecane saturated core samples (106 vertical and 279 horizontal plugs), from seven Meramec wells were acquired. Porosity and mineralogy were also measured on each core plug. We propose two approaches to estimate Vs from Vp: 1) ignoring anisotropy, we combine both Vp and Vs measurements from all vertical plugs and low anisotropy horizontal plugs to create a single systematic, and 2) considering anisotropy, Vp measurements from horizontal plugs were corrected based on the Thomsen's compressional wave anisotropy parameter and the systematics were generated.

The Meramec formation has weak shear wave anisotropy, typically < 10%. Analysis shows that velocities are more sensitive to porosity than mineralogy by a factor of approximately 10. The Vp and Vs dependencies are shown below, for dodecane saturated samples (Ø is the volume fraction pores, C is the weight fraction clay, using vertical and horizontal samples with low anisotropy):

$Vp=6.4-1.5C-15.5\phi$ ($R^2=0.5$)

Vs=3.6-0.9C-5.1ϕ (R^2=0.4)

The shear wave systematics for dodecane saturated measurements are (All velocities are km/s.):

Method 1: Vs= 0.90 + 0.42Vp (R^2=0.7)

Method 2: Vs= 0.20 + 0.56Vp (R^2=0.6)

The first equation has a smaller residual and estimated error than the second equation. Using the first equation, the Meramec velocity systematic shows good agreement with dipole wireline measurements even though there is a substantial difference in measurement frequencies. The Meramec velocity systematics are considerably different from published systematics. Seven Meramec layers can also be grouped into three groups based on the Vp-Vs equations and lithology.

The Meramec shear-wave systematics can be applied in wireline and seismic analyses. The result shows that the method of ignoring anisotropy provides a better Vs estimation than the method considering anisotropy. However, the second method can be potentially applied to a formation that has high anisotropy. Applying Castagna's mudrock equation, using compressional wave velocity to predict shear wave velocities yield an estimation error 6% to 16% in Vs. It is critical to generate specific velocity systematics which are calibrated to the formation of interest.

1 INTRODUCTION

Elastic wave velocities are often used to interpret formation properties, such as porosity, mineralogy, and lithology. Shear-wave velocity (Vs) is potentially useful in unconventional reservoirs for formation evaluation, completion design (Rickman et al., 2008), seismic calibration (Vernik, 2016) and as a lithology discriminator (Pickett, 1963; Aranibar et al., 2013; Tran, 2014). However, legacy shear-wave sonic velocity logs may be few, while compressional wave sonic velocity logs are more common. Therefore, velocity systematics are valuable in creating elastic models when only P-wave logs exists in legacy wells.

A widely used method to generate empirical correlations relating the velocities to rock parameters is laboratory ultrasonic measurements of compressional and shear wave velocities.

Velocities are useful tools for porosity estimation. One of the best-known historical examples is Wyllie's equation (Wyllie, 1956). Wyllie (1957) admitted the physics behind his law was flawed but argued that it seemed to work anyway. Raymer et al. (1980) modified this formula by suggesting different laws for different porosity ranges. These models work for certain rock types, but do not have general applicability.

Velocities also can be used for lithology identification. Pickett (1963) found a useful correlation between mineralogy and the ratio of compressional to shear velocities.

Several attempts have been made to estimate the effect of clay content on acoustic velocities (Tosaya and Nur, 1982; Kowallis et al. 1984; Castagna et al. 1985; Han et al. 1986). These studies have generally found linear correlations relating velocity to both porosity and clay content.

While studying sandstone, siltstone, and silty shale rocks from Cotton Valley and Ardmore Basin, Tosaya and Nur (1982) observed that velocities depend more strongly on porosity than on clay content (by a factor of 3–3.6) in fully saturated rocks. Tosaya (1982) and Castagna (1985) studied the dependence of velocities on clay and porosity in saturated shaly sands, in a limited dataset. Han et al. (1986) adopted a similar approach to study the changes in compressional and shear velocities. The study included a broader siliciclastic sample with conditions varying from well consolidated to poorly consolidated, and from clay-free to shaly sandstones. Compressional and shear velocities were found to correlate linearly with porosity and clay content in shaly sandstones. However, as with Pickett's (1963) results, great care must be taken when extrapolating these correlations beyond the range of samples used to derive them.

Porosity prediction from velocities using Tosaya (1982), Castagna (1985), or Han's (1986) equations requires the accurate estimation of clay content. The clay content was obtained by thin section microscopy, X-ray diffraction, and elemental analysis. The effect of porosity on the velocity is greater than the effect of clay content. To refine the porosity prediction issue in shaly sands, Vernik (1994) developed a petrophysical classification of siliciclastic, which considers the amount of volumetric clay content and the textural position of clay. The compressional velocity versus porosity relations for consolidated rocks in each of the following groups is found to be linear with very high correlation coefficients. The equations are shown as below (brine saturated samples under effective pressure 5800psi):

Clean Arenites, C<2%: $V_p = 6.07 - 7.97\emptyset$ (R^2=0.99) Eq 1-1

Arenites, C=2-15%: $V_p = 5.52 - 6.91\emptyset$ (R^2=0.97) Eq 1-2

Wackes, C=15-35%:	V_p 5.19 − 7.21∅ (R^2=0.96)	Eq 1-3
Shales, C=35%	$V_p = 4.93 - 9.03\emptyset$ (R^2=0.97)	Eq 1-4

Where,

C is clay content, vol%

Vp is compressional wave velocity, km/s

ϕ is fractional porosity

This allows for porosity estimates or lithology prediction in consolidated siliciclastic from acoustic velocities. This classification was also successfully applied in deep-water reservoir Gulf of Mexico turbidities (Vernik, 2002); these are largely unconsolidated sediments.

Shear-wave velocity (Vs) is a potentially useful quantity in unconventional reservoirs for formation evaluation but legacy shear-wave sonic velocity logs are few. Therefore, there are some studies on shear wave velocity prediction. Relationships between compressional and shear wave velocities were established in the classic paper by Pickett (1963) and later by Castagna et al. (1985), Han et al. (1986), etc. Linear trends for correlating the compressional and shear wave velocities are presented, including the Castagna mudrock line derived from *in-situ* sonic and seismic measurements. The work of Brie et al. (1995) extended the work of Castagna et al. (1985) to include predicting gas saturation from a Vp/Vs versus compressional travel time cross plot.

However, in unconventional reservoirs, the Greenberg-Castagna (1992) shear-wave velocity prediction method does not yield accurate shear wave velocities in organic rich unconventional reservoirs, with observed mean errors varying from 6% to 16% (Vernik et al., 2018). Furthermore, Quirein et al. (2015) found that the Castagna mudrock and Brie et al. (1995)

water-wet sand trends do not appear to apply in general to the Eagle Ford, Haynesville, or Barnett mudstone formations due to the presence of carbonates (mainly limestone) and organic matter. Therefore, a better understanding of Vp-Vs relations of unconventional reservoirs is needed.

The focus of this study is the Mississippian Meramec play in Oklahoma. Price et al. (2020) classifies the Meramec formation as a clastic system dominated by siltstone to very-fine–grained sandstone with varying amounts of quartz, clay, and calcareous grains and cement. In this study, a Vs-Vp systematic is developed for the Meramec formation using laboratory pulse transmission ultrasonic measurements. The influences of porosity and mineralogy on velocities are discussed and compared to published velocity systematic and literature systematics is provided.

1.1 Synopsis

The thesis is divided into six chapters and is organized as follows:

Chapter 1 is a brief background and introduction to elastic wave velocities versus reservoir properties, as well as the scope of this study;

Chapter 2 provides the theoretical background to elastic wave velocities and the correlation between elastic velocities and formation properties;

Chapter 3 introduces the geological setting of the study area;

Chapter 4 explains the methodology of the petrophysical measurements performed on the samples;

Chapter 5 lists the petrophysical measurements results and interpretation of the findings, and

Chapter 6 lists the major findings of this research and the application of this study.

2 LITERATURE REVIEW

2.1 Wave propagation

Understanding the elastic properties of rocks is essential in understanding the seismic response to hydrocarbon reservoirs under different environmental conditions. Elastic properties of rocks are dominated by the properties of the solid rock skeleton and "defects" like pores, fractures, and cracks. In most cases, these defects have dimensions smaller than the seismic, sonic, or ultrasonic wavelengths.

There are two basic waves which propagate in a homogeneous isotropic elastic medium: compressional (P-waves) and shear (S-waves). Compressional wave is a wave in which the particle motion is in the direction of the wave propagation. It is called primary waves because it arrives before shear wave. Shear waves split into two orthogonal phase components displaying different velocities as they propagates through an anisotropic medium (**Figure 2.1**). The two components are referred to as a slow and fast shear wave, respectively. Slowness difference between the components depends on the extent of anisotropy. Shear wave splitting is among the most direct and unambiguous indicator of seismic anisotropy (Crampin, 1984; Teanby et al., 2004).

Compressional and shear waves are sensitive to the presence of fractures or cracks when their direction of propagation or their direction of polarization is at an angle to the fracture faces (**Figure 2.2**) (Nur et al., 1969; Rai and Hanson, 1988). Vertically propagating P-waves will not be very sensitive to vertical fractures. S-waves on the other hand have sensitivity to fractures in both horizontal and vertical direction due to their polarization. Vertically propagating shear waves that are polarized parallel to the fracture planes will travel faster than

shear waves polarized perpendicular to the fracture planes. The fractional difference between the velocities of the two shear waves is defined as the shear wave birefringence.

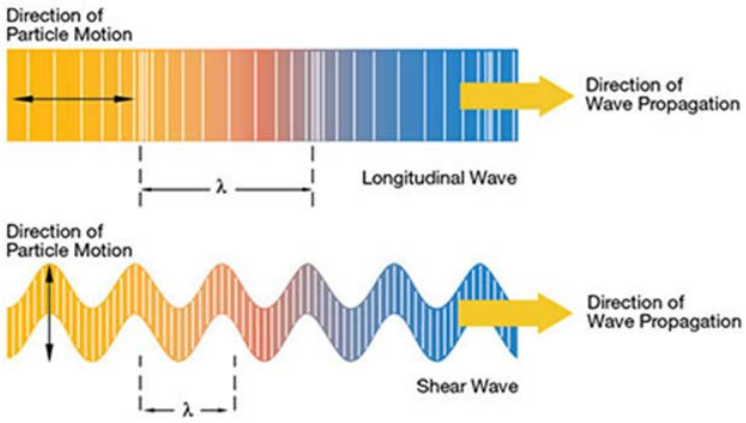

Figure 2.1 P-wave and S-wave propagation (NDT Resource Center, 2017).

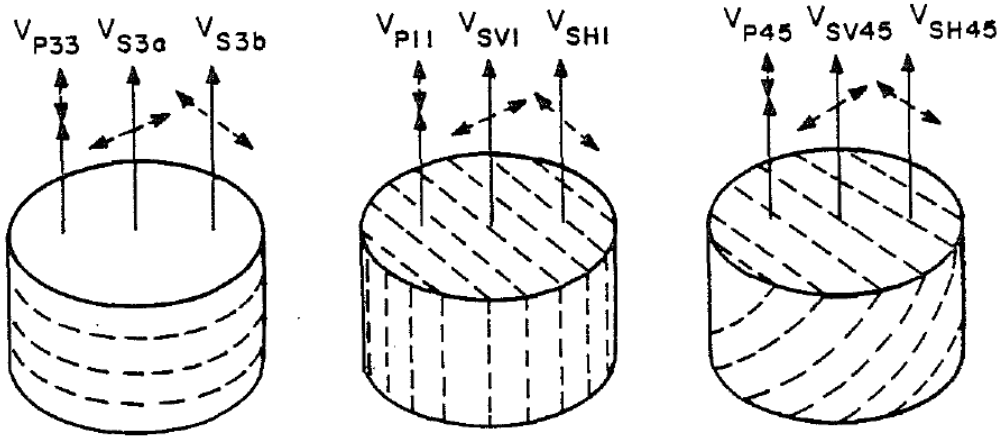

Figure 2.2 Schematic showing P-wave and polarized S-wave propagation through a laminated medium (Lo et al., 1986). In this figure $V_{S3a} = V_{s3b}$ and $V_{SV1} < V_{SH1}$.

Elastic anisotropy means that the stiffness or effective shear moduli in one direction will be different from that in another. For shear waves, their particle motion will be approximately normal to the direction of propagation. The velocity will depend on the orientation of the particle motion. The shear wave can "split" into two shear waves with orthogonal particle motion, each traveling with the velocity determined by the stiffness in that direction. An example of this is shown in **Figure 2.3** from Sondergeld and Rai (1992).

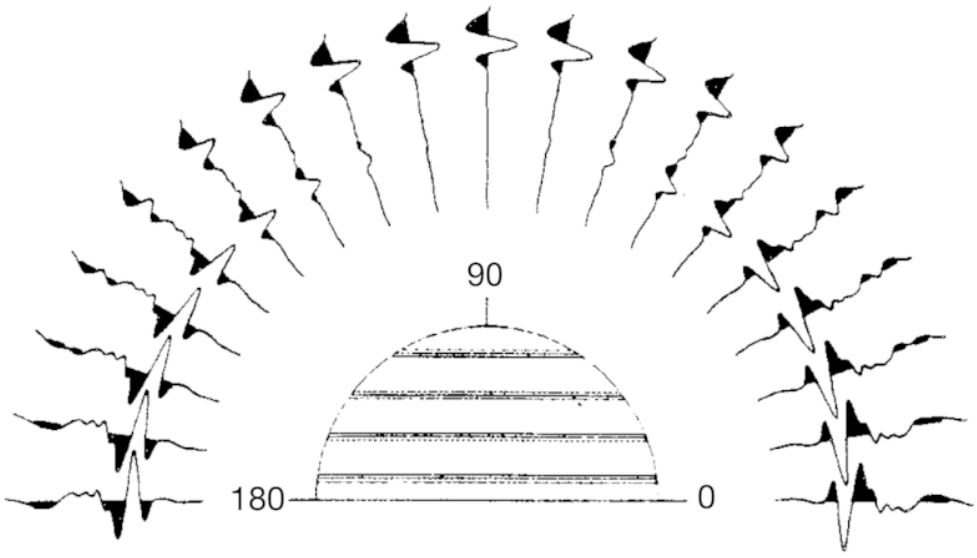

Figure 2.3 Transmitter and receiver are rotated simultaneously through an azimuth aperture of 180°. When particle motion is either parallel or perpendicular to the shale fabric, only one arrival wave is seen. At other angles, both slow and fast waves are present (Sondergeld and Rai, 1992).

2.2 Anisotropy

Rocks, especially shales found in unconventional reservoirs, are generally anisotropic. Shales cover about 60-70% of sedimentary basins (Broichhausen et al. 2005). These clay-rich rocks are important as they form source rocks, seals, and sometimes unconventional reservoirs. These rocks are often elastically anisotropic, as observed in the field (Banik, 1984; Alkhalifah and Rampton, 2001) and laboratory measurements (Jones and Wang, 1981; Lo et al. 1986; Vernik and Nur, 1992; Hornby et al., 1994; Johnston and Christensen, 1995; Wang, 2002; Sondergeld and Rai, 2011). The elastic properties of these rocks - isotropic or anisotropic, are manifestations of the geological processes and the resulting microscopic and macroscopic structures in shale. Elastic anisotropy in these rocks, if not properly accounted for, leads to errors in seismic imaging (Vestrum, et al. 1999) and interpretation, and reservoir

characterization. Thus, it is important to identify and characterize anisotropy to understand and interpret the sonic response of unconventional reservoirs.

The impact of anisotropy in seismic and borehole acoustics was recognized early. Gassmann (1964) presented results dealing with travel-time methods in anisotropic media—in particular, transversely isotropic media. Daley and Hron (1977) computed reflection, transmission, and reflection coefficients in a layered media displaying transverse isotropy. Jones and Wang (1981) measured the velocities of two Cretaceous shales from the Williston basin. They found these samples are transversely isotropic with symmetry axis perpendicular to bedding. The transverse isotropy was due to clay mineral alignment parallel to bedding. White (1982) considered waveform travel in a transversely anisotropic media. Using the ultrasonic measurement for Chelmsford Granite, Chicopee Shale, and Berea sandstone, Lo et al. (1986) found that the elastic anisotropy is due to the combined effects of pores, cracks, and mineral grain orientation. They also observed the crack induced anisotropy decreases with increasing confining pressure.

Thomsen (1986) pointed out that in most cases of interest to geophysicists the anisotropy is weak (<=10 percent) and the weak anisotropy can be characterized by three anisotropy parameters—ε, γ, and δ. The concept has been widely adopted in rock physics to understand and quantitatively characterize anisotropy. This can be explained through the constitutive equations of linear elasticity as:

$$\sigma_{ij} = \sum_{k=1}^{3} \sum_{l=1}^{3} C_{ijkl} \epsilon_{kl} \qquad \text{Eq 2-1}$$

For an isotropic material, the number of independent constants reduces to two and the tensor of elasticity has the form:

$$\begin{vmatrix} c_{11} & c_{12} & c_{12} & 0 & 0 & 0 \\ c_{12} & c_{11} & c_{12} & 0 & 0 & 0 \\ c_{12} & c_{12} & c_{11} & 0 & 0 & 0 \\ 0 & 0 & 0 & c_{44} & 0 & 0 \\ 0 & 0 & 0 & 0 & c_{44} & 0 \\ 0 & 0 & 0 & 0 & 0 & c_{44} \end{vmatrix} \text{ with } c_{12} = c_{11} - 2c_{44} \quad \text{Eq 2-2}$$

The simplest anisotropy case (transverse isotropy) has only one distinct direction (usually vertical) while the other two directions are equivalent. The stiffness matrix thus reduces to 12 non-zero components having five independent components (C_{11}, C_{13}, C_{33}, C_{44}, and C_{66}) as:

$$\begin{vmatrix} c_{11} & c_{11} - 2c_{66} & c_{13} & 0 & 0 & 0 \\ c_{11} - 2c_{66} & c_{11} & c_{13} & 0 & 0 & 0 \\ c_{13} & c_{13} & c_{33} & 0 & 0 & 0 \\ 0 & 0 & 0 & c_{44} & 0 & 0 \\ 0 & 0 & 0 & 0 & c_{44} & 0 \\ 0 & 0 & 0 & 0 & 0 & c_{66} \end{vmatrix} \quad \text{Eq 2-3}$$

This anisotropy is a case of broad geophysical applicability. In this material, Saxena (2018) summarized three modes of wave propagation, and their velocities are dependent on the angle θ between the axis of symmetry (z-axis) and the direction of the wave vector:

Quasi-longitudinal mode $v_P(\theta) = \sqrt{\left(\frac{1}{2\rho}\right)}\sqrt{c_{11}sin^2\theta + c_{33}cos^2\theta + c_{44} + A}$ Eq 2-4

Quasi-shear mode $v_{sv}(\theta) = \sqrt{\left(\frac{1}{2\rho}\right)}\sqrt{c_{11}sin^2\theta + c_{33}cos^2\theta + c_{44} - A}$ Eq 2-5

Pure shear mode $v_{sh}(\theta) = \sqrt{\left(\frac{1}{\rho}\right)}\sqrt{c_{66}sin^2\theta + c_{44}cos^2\theta}$ Eq 2-6

$A = \sqrt{[(c_{11} - c_{44})sin^2\theta + (c_{33} - c_{44})cos^2\theta]^2 + (c_{13} + c_{44})^2 sin^2 2\theta}$ Eq 2-7

In this case, Thomsen (1986) defined the following parameters, P-wave anisotropy ε, S-wave anisotropy γ, and parameter δ:

$$\varepsilon = \frac{c_{11} - c_{33}}{2 \cdot c_{33}} \quad \text{Eq 2-8}$$

$$\gamma = \frac{c_{66} - c_{44}}{2 \cdot c_{44}} \quad \text{Eq 2-9}$$

$$\delta = \frac{(c_{13} + c_{44})^2 - (c_{33} - c_{44})^2}{2 \cdot c_{33} \cdot (c_{33} - c_{44})} \quad \text{Eq 2-10}$$

For the determination of all five tensor elements of a transversely isotropic material, the following five velocities (and the density) can be used: Vp (0°), Vp (90°), Vp (45°), Vsh (90°), and Vsh (0°) = Vsv (0°):

$$c_{11} = \rho \cdot V_p^2(90°) \quad \text{Eq 2-11}$$

$$c_{33} = \rho \cdot V_p^2(0°) \quad \text{Eq 2-12}$$

$$c_{44} = \rho \cdot V_{sh}^2(0°) \quad \text{Eq 2-13}$$

$$c_{12} = c_{11} - 2\rho \cdot V_{sh}^2(90°) \quad \text{Eq 2-14}$$

$$c_{13} = \sqrt{4\rho^2 \cdot V_p^4(45°) - 2\rho^2 \cdot V_p^4(45°) \cdot (c_{11} + c_{33} + 2c_{44}) + (c_{11} + c_{44}) \cdot (c_{33} + c_{44})} - 2c_{44} \quad \text{Eq 2-15}$$

Many studies have been done to understand the correlation between reservoir properties and anisotropy. Anisotropy results from the organized distribution of platy clay minerals (Hornby et al. 1994; Johnston and Christensen, 1995; Sondergeld and Rai, 2011). There is a strong positive correlation between the degree of preferred orientation of clay mineral alignment and seismic anisotropy. Another cause of anisotropy is the existence of compliant organic materials (Vernik and Nur, 1992; Vernik and Liu, 1997; Sondergeld et al. 2000; Vernik and Milovac, 2011). Several studies of some kerogen rich shales show that the anisotropy of the shales is related to the kerogen content and maturation level (Vanorio et al. 2008; Ahmadov, 2011).

Berryman (2008) analyzed the approximations involved in Thomsen's weak anisotropy approach and extended the original model to the case of strong anisotropy. While Thomsen's approximation suggests these velocities as completely symmetric around θ=π/4=45degrees,

this generally is not true of the actual wave speeds. Berryman suggested a new set of equations for strong anisotropy to define velocities as:

$$v_P \cong \alpha_0 \left[1 + \varepsilon sin^2\theta - (\varepsilon - \delta)\frac{2sin^2\theta_m sin^2\theta cos^2\theta}{[1 - cos2\theta_m cos2\theta]}\right] \quad \text{Eq 2-16}$$

$$v_{sv} \cong \beta_0 \left[1 + \frac{\alpha_0^2}{\beta_0^2}(\varepsilon - \delta)\frac{2sin^2\theta_m sin^2\theta cos^2\theta}{[1 - cos2\theta_m cos2\theta]}\right] \quad \text{Eq 2-17}$$

α_0 and β_0 are vertical P-velocity and S-velocity, respectively. The parameter θ_m is defined by:

$$tan^2(\theta_m) = \frac{(c_{33} - c_{44})}{(c_{11} - c_{44})} = \frac{v_p^2(0) - v_s^2(0)}{(1 + 2\varepsilon)v_P^2(0) - v_s^2(0)} \quad \text{Eq 2-18}$$

2.3 Parameters that affect velocities:

2.3.1 Porosity

Wyllie et al. (1956) derived their famous time–average equation relating porosity and compressional velocity:

$$\frac{1}{V_p} = \frac{1 - \emptyset}{V_{p,ma}} + \frac{\emptyset}{V_{fl}} \quad \text{Eq 2-19}$$

Where,

V_p is the compressional wave velocity of the porous rock,

$V_{p,ma}$ is the compressional wave velocity of the matrix material,

V_{fl} is the compressional wave velocity of the pore fluid

Rearranging a linear relationship between measured compressional wave slowness (10^6/Vp, usec/ft), and porosity results in the equation:

$$\emptyset = \frac{\Delta t_P - \Delta t_{P,ma}}{\Delta t_{fl} - \Delta t_{P,ma}} \quad \text{Eq 2-20}$$

Where,

Δt_P is the compressional wave slowness of the porous rock,

$\Delta t_{P,ma}$ is the compressional slowness of the matrix material,

Δt_{fl} is the compressional slowness of the pore fluid.

It may be noted that the Wyllie equation is heuristic and not a model derived equation (the addition of travel time for matrix and fluid is physically valid only for wavelengths much smaller than pore or grain size). The equation only pertains to compressional velocities. The equation works best for water-saturated and well-compacted porous rocks, particularly sandstones. In shaly sandstones and shales, the time average equation significantly overestimates velocities (De Martini et al. 1976; Tosaya and Nur, 1982; and Kowallis et al. 1984). Presence of gas can also give erroneous results (Asquith and Krygowski, 2004).

Under poor consolidation or low effective stress condition, the high slowness values will cause an overestimated of porosity. Therefore, a compaction correction is necessary in this case. Raymer et al. (1980) provided compaction-corrected Wyllie porosity equation (slowness in an adjacent shale bed is used as compaction reference, $\Delta t_{shale} > 100 \mu s ft^{-1}$):

$$\emptyset_{corrected} = \emptyset_{Wyllie} \cdot \frac{1}{C_P} = \frac{\Delta t_P - \Delta t_{ma}}{\Delta t_{fl} - \Delta t_{ma}} \cdot \frac{100}{\Delta t_{shale}} \quad \text{Eq 2-21}$$

In sandstones with porosity less than 0.37, Raymer et al. (1980) derived the following equation, known as the Raymer–Hunt–Gardner equation:

$$V_P = (1 - \emptyset)^2 \cdot V_{P,ma} + \emptyset \cdot V_{fl} \quad \text{Eq 2-22}$$

Jennings and Lucia (2001) discussed the influence of pore type with respect to Wyllie's equation. They point out that in the absence of vuggy pore space, limestones typically follow the Wyllie time–average equation, although the scatter can be quite large. When grain-mold or intra-fossil pore space is present, the data deviates from the Wyllie equation. This can be described empirically by implementation of separate vuggy porosity (Lucia, 2007).

2.3.1 Mineralogy

Mineralogy affects rock velocities in two ways. The most obvious is through the bulk and shear moduli of the solid matrix, which are primary inputs to all velocity models. Indirectly, mineralogy controls the cementation and the pore structure of the rock. Other parameters being equal, silica and carbonate cements produce higher velocities than clay cement. Carbonates, being more soluble, often have extremely complex pore structures which are not well described by conventional velocity models.

Pickett (1963) found a useful correlation between mineralogy and the ratio of compressional to shear velocities. In more poorly consolidated rock, the data tend to diverge from the trends and many empirical alternatives have been proposed, e.g. Castagna, 1993.

Tosaya and Nur (1982) investigated the dependence of compressional velocities in detrital silicate rocks on porosity, volume of clay and clay mineralogy. Eighteen samples with porosity range from 4.2% to 20% and total clay volume varied from less than 1% to 72%. The clay content was obtained by thin-section microscopy, X-ray diffraction, and elemental analysis. Velocities were measured in low-salinity brine and water saturated samples. They concluded that P-wave velocity depends on porosity more strongly than on clay content by a factor of 3.6

and the Vp-porosity-clay equation for these 18 samples is (velocities in km/sec, porosity is the volume fraction pores, and clay is the volume fraction clay):

$$V_p = -2.4C - 8.6\emptyset + 5.8 \quad \text{Eq 2-23}$$

However, this was a preliminary study which required confirmation and refinement.

Following the lead of Tosaya (1982), Castagna et al. (1985) used multiple linear regression to determine the dependence of sonic derived compressional and shear wave velocity on porosity and clay content for the Frio Formation. The porosity and volume of clay are determined from gamma ray, neutron, and density logs. The equations are shown below (velocities in km/sec, porosity is the volume fraction pores, and clay is the volume fraction clay):

$$V_p = 5.81 - 9.42\emptyset - 2.21C \quad \text{Eq 2-24}$$

$$V_s = 3.89 - 7.07\emptyset - 2.04C \quad \text{Eq 2-25}$$

Han (1986) confirmed the correlation between velocities and clay content using a larger set of samples. 75 sandstone samples with porosity range from 2 to 30 percent and clay content by volume fraction ranging from 0 to 50 percent. The samples were brine saturated. The result shows that the effects of porosity and clay content on the shear wave velocity are larger than on the compressional wave velocity. The effect of porosity on velocity change is about 3 times compared to the effect of clay content on velocity change. Both porosity and clay content have a stronger effect on P-wave velocity than S-wave velocity. The equations are shown below (velocities in km/sec, porosity is the volume fraction pores, and clay is the volume fraction clay, at confining pressure of 40 MPa and pore pressure of 1 MPa):

$$V_p = 5.59 - 6.93\emptyset - 2.18C \quad \text{Eq 2-26}$$

$$V_s = 3.52 - 4.91\emptyset - 1.89C \quad \text{Eq 2-27}$$

Marion and Jizba (1992) have investigated North Sea shaly sand reservoir rocks (35 MPa pressure) for brine and gas saturation and derived the regressions (velocities in km/sec, porosity is the volume fraction pores, and clay is the volume fraction clay):

Gas saturation:

$$V_p = 4.82 - 5.02\emptyset - 0.597C \quad \text{Eq 2-28}$$

$$V_s = 3.26 - 3.03\emptyset - 0.952C \quad \text{Eq 2-29}$$

Brine saturation:

$$V_p = 5.46 - 6.29\emptyset - 1.10C \quad \text{Eq 2-30}$$

$$V_s = 3.32 - 3.62\emptyset - 0.952C \quad \text{Eq 2-31}$$

Kirchberger (2001) analyzed logging data from the Vienna Basin and used the gamma log for characterizing the shale content, vshale, and the density log for porosity estimate. Shaly sand formations (water bearing) follow a regression (velocities in km/sec, porosity is the volume fraction pores, and clay is the volume fraction clay):

$$V_p = 5.358 - 5.402\emptyset - 2.926C \quad \text{Eq 2-32}$$

$$V_s = 2.802 - 3.935\emptyset - 1.750C \quad \text{Eq 2-33}$$

These studies have generally found linear correlations relating velocity to both porosity and clay content. Generally, it is found that the velocities are more sensitive to porosity than clay content. However, great care must be taken when extrapolating these correlations beyond the range of samples used to derive them. As clay content increases, sandstones grade into shaly sands and shales. A transition occurs from a grain supported framework with clay in the pore space, to a clay matrix with embedded, isolated grains.

2.3.2 Effect of pressure and temperature

At a given pressure and temperature, the velocity of sedimentary rocks depends on rock properties, such as porosity, cracks, pore fluid content, and lithology. In order to relate velocities to rock properties, the effects of pressure and temperature on velocities need to be understood.

Simmons and Brace (1965) have shown that Vp and Vs measured for a rock sample can vary significantly depending on the effective pressure. Many laboratory measurements also show that most rocks obey the effective stress law:

$$P_{eff} = P - \alpha \cdot P_{pore} \qquad \text{Eq 2-34}$$

Where,

P_{eff} is the effective pressure

P is the total external pressure

P_{pore} is the pore pressure

α is Biot-Willis parameter depending on material compressibility. $\propto = 1 - K_*/K_o$ (where K_*= the bulk modulus of the porous rock frame (drained of any pore-filling fluid), K_o=the bulk modulus of the mineral matrix)

When α is equal to 1, the effective pressure is equal to the difference between confining and pore pressure, which is differential pressure. Increasing confining pressure or decreasing pore pressure cause velocities to increase. In general, there is a characteristic non-linear dependence of velocity on depth or pressure (Domenico, 1976). In most cases, wave velocities increase strongly with increasing pressure at low levels, and less at high pressure.

The increase in velocity with pressure is usually attribute to two reasons, grain contacts within the rock and closing of crack-like pores. As stress increases, the grain contacts become stiffer, as does the entire frame (Birch, 1960; Birch, 1961; Digby, 1982; Murphy, 1984; Murphy, 1986). This approach has been utilized in several theoretical models (Kuster and Toksoz, 1974; O'Connell, 1974; Mavko, 1978; Cheng, 1979).

The dependence of velocity on effective pressure makes the velocity-porosity relationships more complicated. Because the pore volume is changing with the effective pressure. Therefore, any velocity-porosity transform must be used very carefully, especially when the transform does not explicitly include pressure as a variable.

The effect of temperature on velocities is small in reservoirs. Geothermal gradients range from about 8 to 40 $^{\circ}$C/km and are typically around 20 $^{\circ}$C /km in many sedimentary basins (Gretener, 1981). Timur (1977) has shown that the velocities drop by only a few percent for a temperature increase of 100 degree Celsius. Kern et al. (2001) also shown that the velocity decreased by a few percent when the temperature increases from room temperature up to 600 degree Celsius under high confining pressure (600MPa). Based on Nur and Simmons (1969) and DeVilbiss et al. (1979), this velocity change is mainly due to the effects of temperature on the pore fluids while the skeleton properties remain approximately constant. A large velocity change can be expected when high temperatures cause a vapor phase, such as steam flooding.

2.4 Vp-Vs relation

The ratio of Vp and Vs is an important property for seismic applications. In order to estimate shear wave velocities when only compressional wave velocities are available, Castagna et al. (1985) derived an empirical equation using *in-situ* sonic and field seismic measurements in mudrock. It is commonly referred to as the "mudrock-line":

$$V_p = 1.16 \cdot V_s + 1.36 \qquad \text{Eq 2-35}$$

Where the velocities are in km/s.

Many researches have published variants of the Castagna mudrock equation. In 1993, Castagna et al. compiled an analysis of data for different sedimentary rocks. Mavko et al. (2020) lists a selection of the modified equation, shown in table:

Table 2-1 Linear Regressions Vs-Vp (km/s) for Sandstone and Shale (Brine-Saturated)

Rock	Equation	Effective Pressure	References
Sandstone	$V_s = 0.804 \cdot V_p - 0.856$	20-50MPa	Castagna et al. (1985) and Castagna (1993)
Shale	$V_s = 0.770 \cdot V_p - 0.867$	20-50MPa	
Shaly sandstone	$V_s = 0.794 \cdot V_p - 0.787$	40 MPa	Han et al. (1986)
Sandstone, clay content > 0.25	$V_s = 0.842 \cdot V_p - 1.10$	40 MPa	
Sandstone, clay content < 0.25	$V_s = 0.754 \cdot V_p - 0.657$	40 MPa	

Sandstone, porosity > 0.15	$V_s = 0.756 \cdot V_p - 0.662$	40 MPa	
Sandstone, porosity < 0.15	$V_s = 0.853 \cdot V_p - 1.137$	40 MPa	

In unconventional formations, organic-rich shales exhibit Vp/Vs ratios that are significantly lower than lithologically similar fully brine-saturated shales having low organic content. Sonic-log measurements of compressional and shear-wave velocities in seven organic-rich shale formations deviate significantly (typically more than 5%) from the Greenberg-Castagna empirical brine-saturated shale trend towards lower velocity ratios (Omovie and Castagna, 2019). The Vp/Vs computed from bedding normal ultrasonic velocity measurements performed by Johnston and Christensen (1995) in an organic-rich New Albany Shale (Illinois Basin, exposed in a southern Indiana quarry) core samples have Vp/Vs ratios as low as 1.48. Acoustic measurements performed by Vernik and Liu (1997) indicate bedding normal organic-rich Bakken shale core samples have Vp/Vs ratios as low as 1.59. Similar low velocity ratios have been observed in ultrasonic velocity measurements performed in a variety of organic rich shales (Omovie and Castagna, 2017; Gong et al. 2018). Possible explanations are the presence of solid kerogen in these shale formations (Vernik and Milovac, 2011; Tran, 2014; Sayers et al. 2015; and Vernik et al., 2018) and/or mechanical effect of free hydrocarbon fluids (Lucier et al. 2011; Omovie and Castagna, 2017), or some combination of the two. Omovie and Castagna (2019) found that the lower Vp/Vs ratio observed in dry, gas-saturated or oil-saturated shales when compared to fully brine-saturated shales, organic and inorganic, can be explained for the most part by the presence of gas or oil.

Quirein et al. (2015) investigated both the laboratory and log based Vp and Vs relations in unconventional formations. They present plots of laboratory data from the Bakken, Bazhenov, Barnett, Eagle Ford, Haynesville, Monterey, and Niobrara organic shales. They also include an investigation of *in-situ* well log data from the Eagle Ford, Haynesville, and Barnett formations in the context of the Castagna, Brie, and additional cross plots. The result shows that the Castagna mudrock and Brie water-wet sand trends do not appear to apply in general to the Eagle Ford, Haynesville, and Barnett mudstone formations. This is attributed to the presence of carbonates (mainly limestone) and organic matter.

Vernik et al. (2018) also found that in unconventional reservoirs with significant organic content, the Greenberg-Castagna (GC) S-wave velocity prediction method (Greenberg and Castagna, 1992) does not yield accurate S-wave velocity predictions. The observed mean errors using Greenberg-Castagna (GC) equation (Greenberg and Castagna, 1992) varies from 6% to 16% in a variety of unconventional reservoirs rich in organic content. Vernik et al. (2018) state that the main factors controlling the bedding-normal P- and S wave velocities and their ratio is the bulk content of the porous organic matter. Considering the total organic carbon content and all the variables that control elastic properties of organic mudrock reservoirs, Vernik et al. (2018) provide two methods to predict Vs in organic rich shale formations and applied to Bakken, Woodford, Avalon, Eagle Ford, Wolfcamp, Cline, and Marcellus. The prediction error between estimated Vs and measured Vs is less than 3%.

All of these correlations are purely empirically and valid only for a specific formation.

3 GEOLOGICAL SETTING

The Anadarko Basin is an asymmetrical foreland basin that trends to the northwest across Oklahoma, Texas Panhandle, southwestern Kansas, and southeastern Colorado (Beebe, 1959; Lane and De Keyser, 1980; Gutschick and Sandberg, 1983; Perry, 1989; Ball et al. 1991). The focus of this study is the Mississippian Meramecian play, which is an emerging North American unconventional oil and gas target in the Anadarko Basin in west central Oklahoma. The region of the study area is shown in the **Figure 3.1** (Price, 2020).

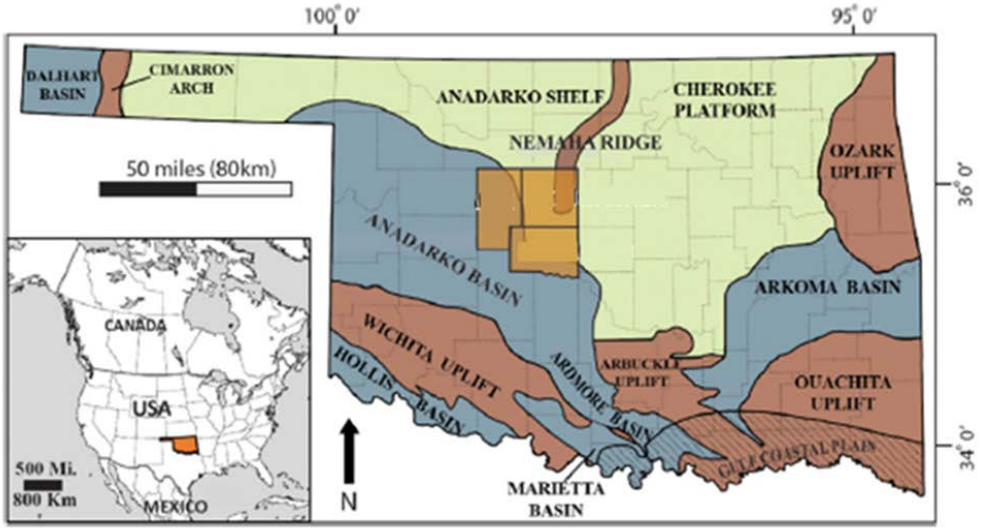

Figure 3.1. Geological provinces of Oklahoma. Study area is highlighted in orange. The Sooner trend is located on the northeastern shelf of the Anadarko Basin (modified from Northcutt and Campbell, 1996).

Mississippian deposits have been divided into four depositional episodes of Kinderhookian, Osagean, Meramecian, and Chesterian age (Northcutt et al. 2001), shown as **Figure 3.2**. The Meramecian play ranges in thickness from 0 to 180 m (0–600 ft). The section thins to the northeast and is absent along the Nemaha ridge. Thickening is observed toward the basin-depocenter to the southwest. To the northwest, the unit thins and pinches out, whereas to the southeast, the section thins and becomes condensed (Price, 2020), as shown in **Figure 3.3**.

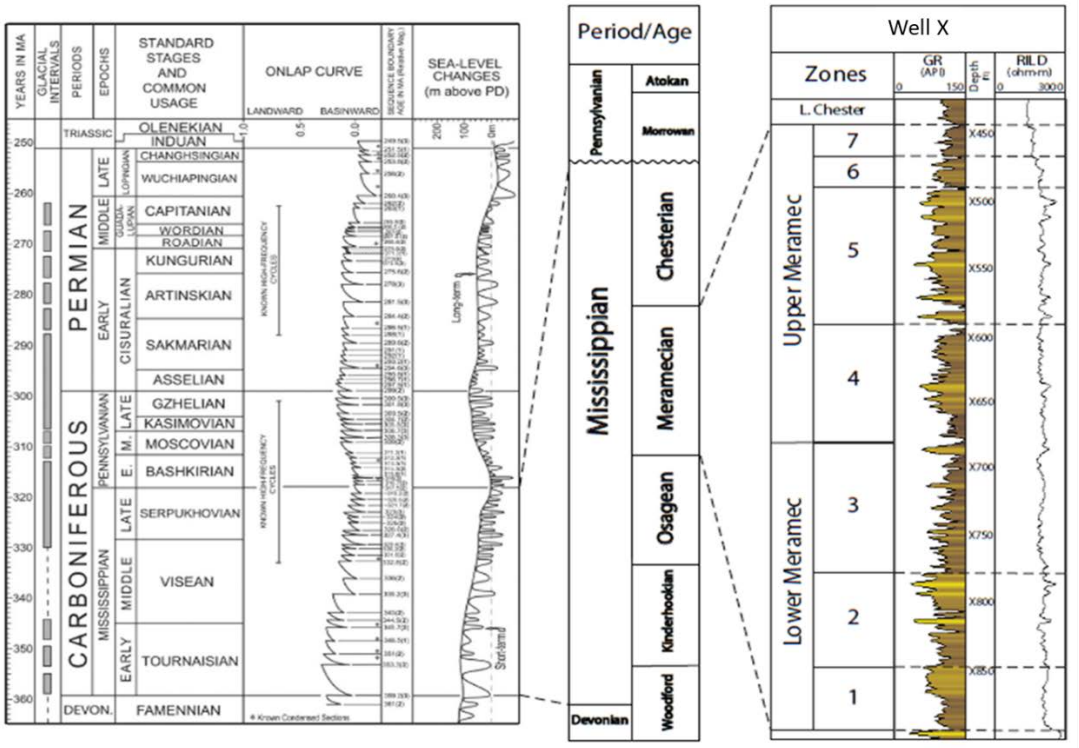

Figure 3.2 Mississippian stratigraphic column is displayed next to the sea level cyclicity of the Carboniferous and Permian periods. The Meramec is deposited during increasing cyclicity due in part to the climatic transition of the Mississippian, resulting in complex stacking patterns and lateral distribution of facies. (Modified from Boyd, 2008; Haq and Schutter, 2008; Miller, 2019; Hardisty, 2019).

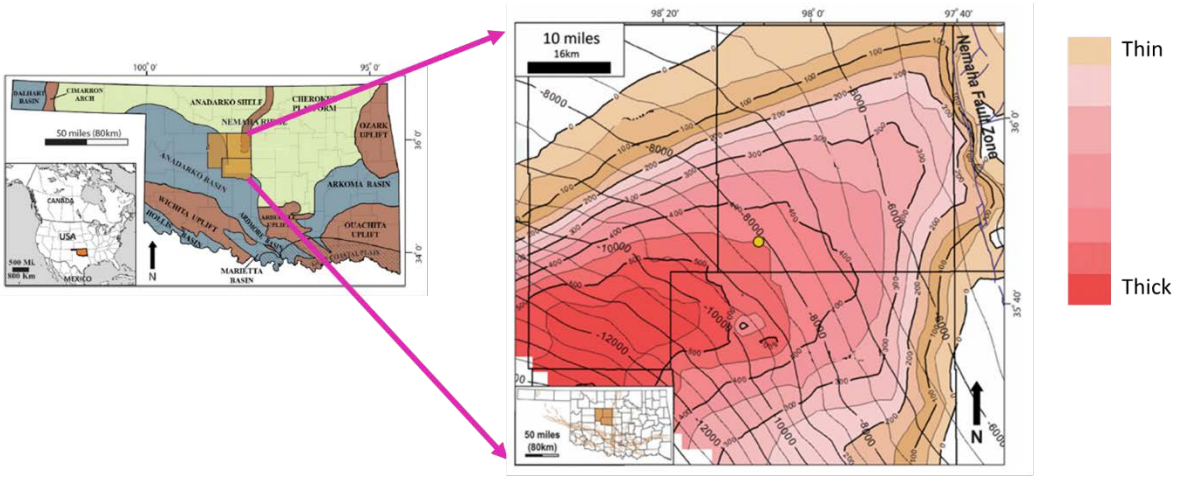

Figure 3.3 Isopach thickness of the Meramecian play interval (color-filled contours) and subsea structure depth to the top of the play (black contours). Faults along the Nemaha Ridge are labeled in blue. Isopach contour interval = 50 ft (15 m); structure contour interval = 250 ft (75 m); yellow dot = type log location (modified from Northcutt and Campbell, 1996; Price, 2020).

The Meramecian play comprises a clastic system dominated by siltstone to very-fine-grained sandstone with varying amounts of quartz, clay, and calcareous grains and cement. (Price, 2020). Price concluded calcite cement to be the primary driver of reservoir quality, attributing the preservation of primary porosity to be a key role of clay within the Meramec. Hardwick (2018) shows the microfacies and the Meramec formation is classified to peloidal calcareous siltstone, calcitic siltstone, siltstone, and argillaceous siltstone. Much of the calcite is in the form of skeletal fragments as opposed to calcite cement due to the increase in clay volume decreasing primary porosity for early calcite cementation. There are lesser amounts of dissolved feldspars as compared to the calcitic siltstone facies, but an additional slot-pore is observed in clay. Therefore, Hardwick (2018) concludes that calcite-cement in Meramecian siltstones significantly obstructed porosity and can act as a seal, while clay-filled matrices provided preservation of primary porosity. Drummond (2018), Hickman (2018), and Miller (2019) identified lithofacies from cores within the Meramec that were composed of a mixed siliceous-calcareous siltstones and heavily bioturbated and laminated mudstones with stacking patterns that indicate shallowing upward cycles capped by flooding surfaces.

4 EXPERIMENTAL METHODOLOGY

Petrophysical measurements were done in the Integrated Core Characterization lab (IC^3). Different properties measured in this study were porosity, Vp, Vs, and mineralogy. A summary of all the measurements is presented in **Figure 4.1**.

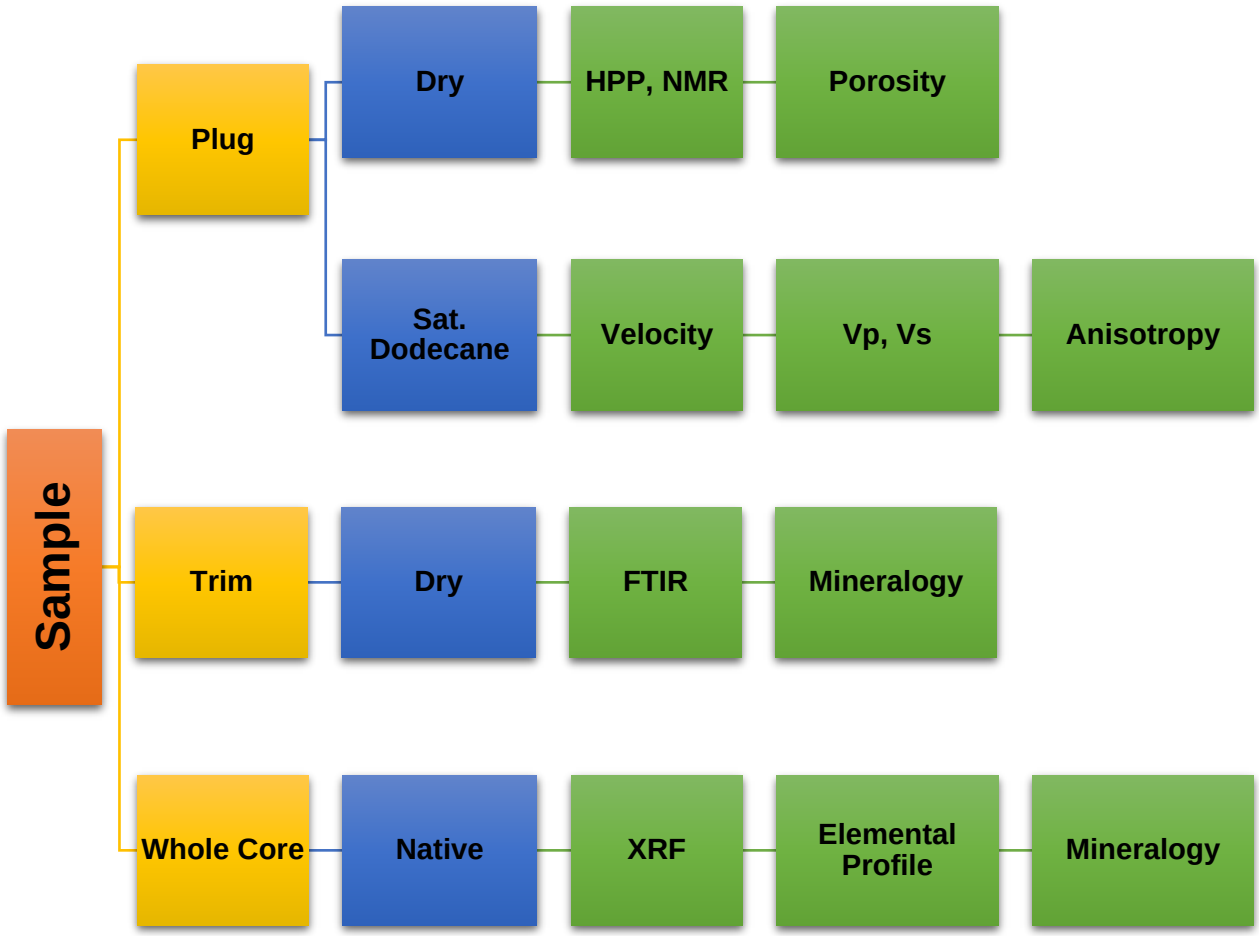

Figure 4.1 Chart showing all the lab measurements performed on the samples used in this study.

4.1 Porosity measurements

Porosity measurements in this study consist of a combination of helium porosity measured on dry samples and an NMR porosity measurement. The helium resolves all the vacant pore space

and the NMR captures the fluid remaining in the pore space. The sum of the two yields a total porosity.

Helium porosity measurement technique is based on the principle of Boyle's Law. The well-polished plug samples are dried at 100 ˚C until the weight is stabilized. After a sample's weight is constant it was put into the desiccator for 30 minutes to cool down to room temperature. The bulk volume is measured using mercury immersion technique. Porosity was measured using high pressure helium pycnometer.

NMR measurements were performed on same core plugs using a 12 MHz OXFORD MARAN Ultra NMR analyzer with Green Imaging Technology acquisition and processing software. A Carr-Purcell-Meiboom-Gill pulse sequence is used to measure the transverse relaxation time (T_2) and the echo spacing is 114 μs.

4.2 Mineralogy measurements: FTIR and XRF

The mineralogy of plug samples was determined using transmission Fourier Transform Infrared Spectroscopy (FTIR). Different minerals have different absorbance spectra signatures. The inversion package, i.e. absorbance spectra to mineralogy, was developed in IC[3]. This technique can identify sixteen minerals: quartz, calcite, dolomite, aragonite, siderite, oligoclase, albite, orthoclase, illite, chlorite, kaolinite, smectite, mixed-layer clays, apatite, anhydrite, and pyrite. Particularly in shales, FTIR gives better quantitative clay volume measurement (Sondergeld and Rai 1993; Ballard 2007). The moisture and organic carbon exhibit strong peaks in the mid-infrared region, which masks the absorption peaks of other minerals. Therefore, the samples were ashed in low temperature plasma asher to oxidize organics prior to measurement.

We used handheld X-Ray fluorescence (XRF) to determine elemental content which was subsequently inverted for mineralogy. The model of the handheld XRF machine is TRACER 5i^{TM} from Bruker. The inversion package from element to mineral was developed in IC^{3}. The measurement was been done on whole core and the spatial resolution is 2-inches (Han et al., 2019).

4.3 Ultrasonic measurements

The dry ultrasonic measurements of selected samples and dodecane saturated ultrasonic measurements of all samples were obtained. To minimize any rock-fluid interaction that could results in shear weakening/strengthening which could affect the velocity measurements (Baechle et al. 2009), dodecane is selected as saturation fluid. The plug samples were subjected to vacuum for 24 hours. Samples were saturated over three pressure steps to minimize inducing cracks. First, the pressure was set at 1000 psi for an hour, then the pressure was raised to 3000 psi for another hour. Finally, the pressure was raised to 5000 psi for 24 hours.

Pulse transmission technique (Mattaboni and Schreiber, 1967) is used for ultrasonic velocity measurements. The velocity measurement configuration is shown in **Figure 4.2**. Each sample is placed between two endcaps, wrapped with a rubber boot, and sealed with hose clamps. The rubber boot provides a seal between sample and the pressurizing oil. The confining pressure steps were from 250 psi to 4500 psi. Each end cap houses three piezoelectric transducers (one compressional and two polarized shear) with a resonance frequency of 1MHz. The piezoelectric crystals generate compressional (P) and two orthogonally polarized shear waves (S1 and S2). The waveforms are recorded at each pressure step and the first arrival time is picked as shown in **Figure 4.3**. Knowing the sample length and first arrival time, the compressional wave velocity, and fast and slow shear wave velocities are calculated.

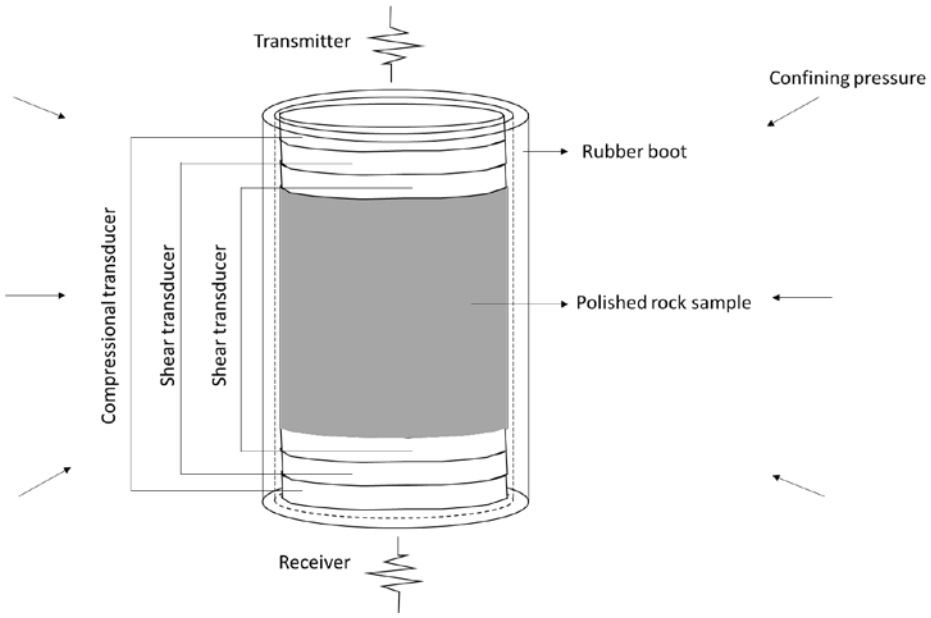

Figure 4.2 Velocity measurement setup. The sample is placed between two endcaps and wrapped with a rubber boot. The rubber boot provides a seal between sample and pressurizing oil. Uniform confining pressure is provided by oil. Computer controlled switching allows sequential activation of the P-wave and two polarized shear wave transducers.

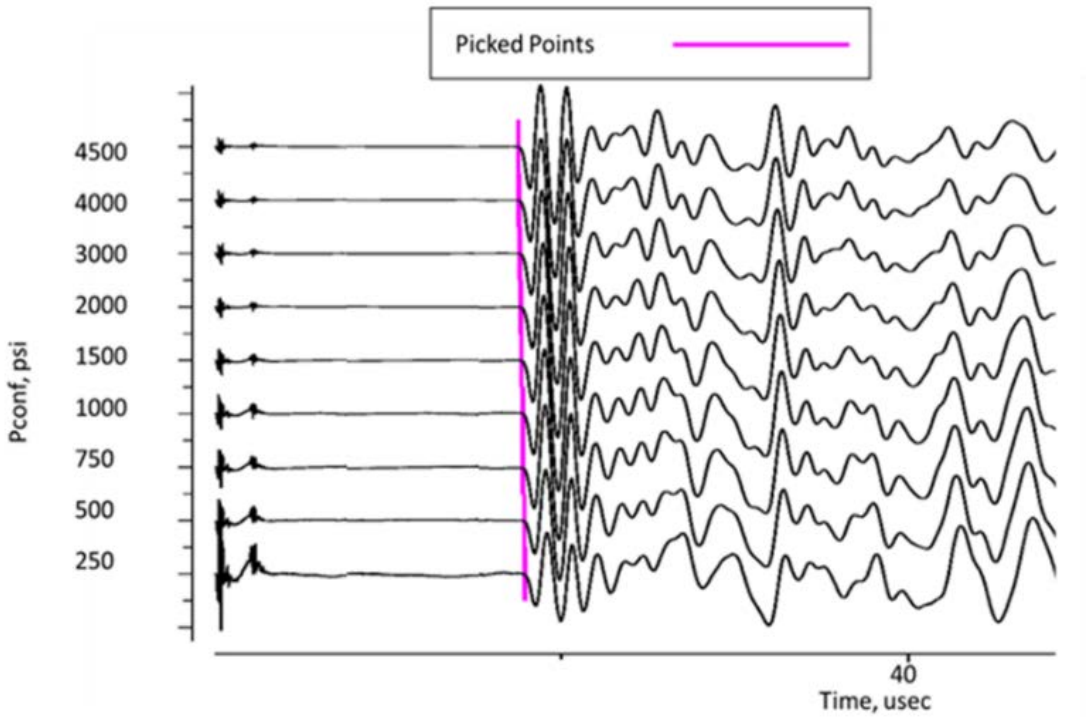

Figure 4.3 Example of the picked arrival time of P-wave. Waveforms are acquired at each confining pressure step. The first arrival time is shown as a pink line.

5 RESULTS AND DISCUSSION

5.1 Sample description

Well locations are shown in **Figure 5.1**. A summary of the samples from each well is shown in **Table 5-1**. There are more horizontal samples than vertical samples. In total, 106 vertical samples and 279 horizontal samples were tested. Among all the samples, 12 pairs of vertical and horizontal samples are cored from the same depth.

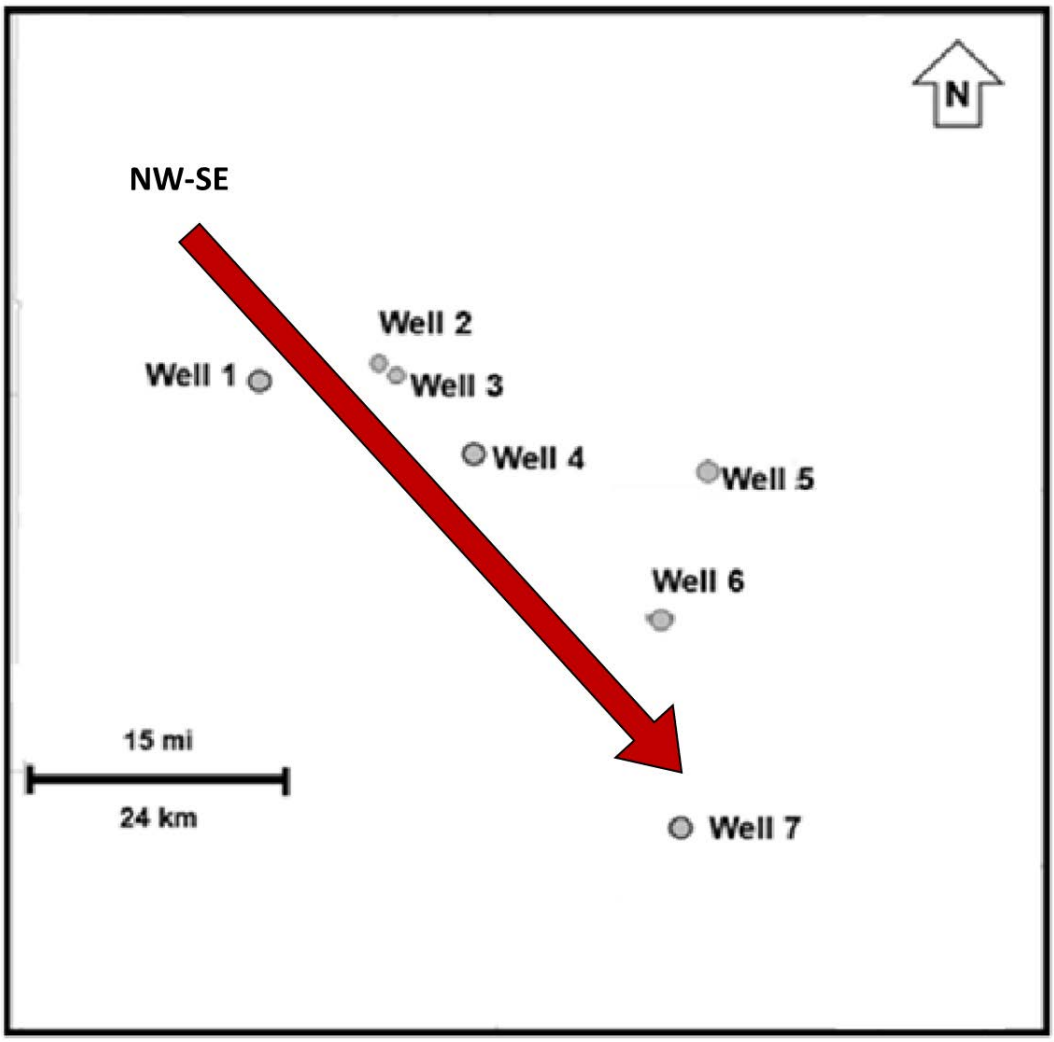

Figure 5.1 Map of wells in the study area. Seven wells are included in this study and the depositional trend of the study area is NW-SE. Wells are named following the depositional trend.

Table 5-1 Summary of sample numbers

Well name	Number of vertical samples	Number of horizontal samples	Number of paired samples (Δρ<5%)
Well 1	0	56	-
Well 2	4	16	2
Well 3	3	13	1
Well 4	59	93	5
Well 5	13	16	-
Well 6	6	57	1
Well 7	21	28	3
SUM	106	279	12

5.2 Anisotropy

Velocity measurements on vertical and horizontal plugs were used to analyze anisotropy, as shown in **Figure 5.2**. From horizontal samples, Vp_horiztontal, Vs_fast (polarized parallel to the bedding plane), Vs_slow (polarized perpendicular to the bedding plane) were measured. From vertical samples, Vp_vertical, Vs_slow (propagating perpendicular to the bedding plane) were measured. The measurements of compressional and polarized shear velocities provide the four elastic constants.

Knowing the Vp parallel and perpendicular to bedding and the fast and slow Vs, two of Thompson's anisotropy parameters can be calculated using Eq 5-1 and Eq 5-2 (Thomsen, 1986). Shear wave anisotropy parameter (γ) requires Vs_fast and Vs_slow measured on horizontal samples. P-wave anisotropy parameter (ε) requires Vp_horizontal and Vp_vertical acquired from horizontal and vertical samples from the same depth.

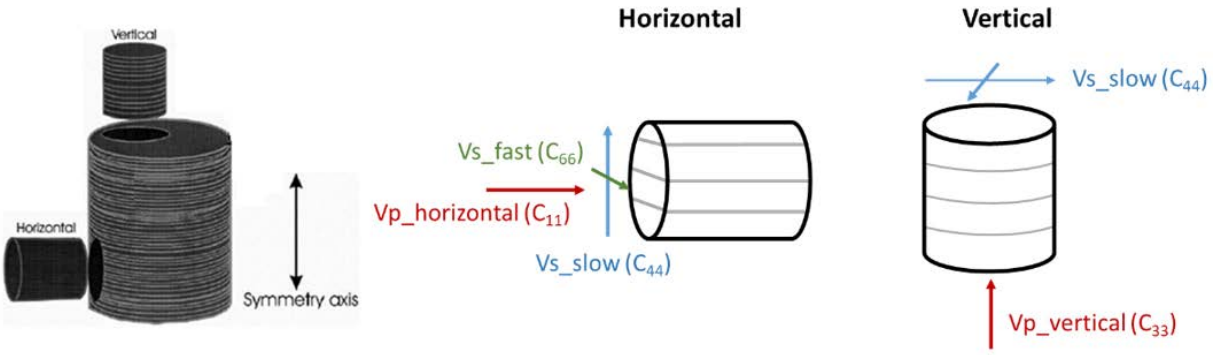

Figure 5.2 Velocity measured from different orientations. Vp_horiozntal, Vs_fast, and Vs_slow are be measured from horizontal plugs. Vp_vertical and Vs_slow are measured on vertical plugs. Bedding planes are shown as grey lines. Propagation directions are red arrows, while the green and blue arrows indicate shear wave polarization directions.

$$\gamma = \frac{C_{66}-C_{44}}{2*C_{44}} = \frac{V_{s\_fast}^2-V_{s\_slow}^2}{2*V_{s\_slow}^2} \quad \text{Eq 5-1}$$

$$\varepsilon = \frac{C_{11}-C_{33}}{2*C_{33}} = \frac{V_{p\_horizontal}^2-V_{p\_vertical}^2}{2*V_{p\_vertical}^2} \quad \text{Eq 5-2}$$

Where,

Vs_slow: slow shear wave velocity (km/s)

Vs_fast: fast shear wave velocity (km/s)

Vp_horizontal: horizontal compressional wave velocity (km/s)

Vp_vertical: vertical compressional wave velocity (km/s)

γ: shear wave anisotropy parameter

ε: compressional wave anisotropy parameter

Anisotropy parameters are calculated using the saturated velocity data measured at 4000 psi, as shown in **Figure 5.3**. Since ε requires a horizontal and a vertical sample from the same depth, there are few data in the box plot. More than 90% of samples have anisotropy parameter, ε and

γ, values less than 0.1 (see **Figure 5.3**). If the anisotropy parameter less than 0.1, the samples can be considered to have "weak" anisotropy (Sondergeld and Rai, 2011). Therefore, the plug samples from Meramec formation can be considered weakly anisotropy or even isotropic. The low anisotropy also supported by SEM images that there is no strong orientation of grains in Meramec formation, as shown in **Figure 5.4**.

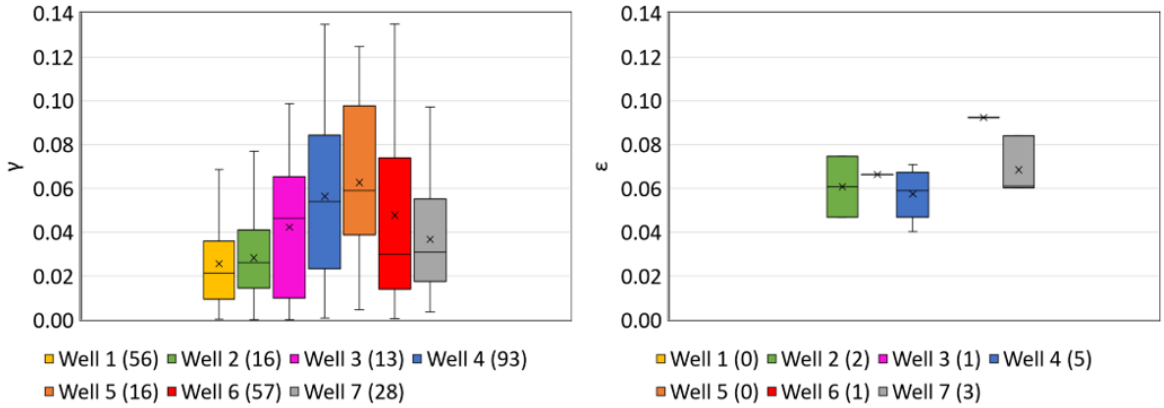

Figure 5.3 Thomsen's anisotropy parameters, ε and γ, of all samples. Number of samples for each well are shown in the brackets. More than 90% of samples have anisotropy values of less than 0.1.

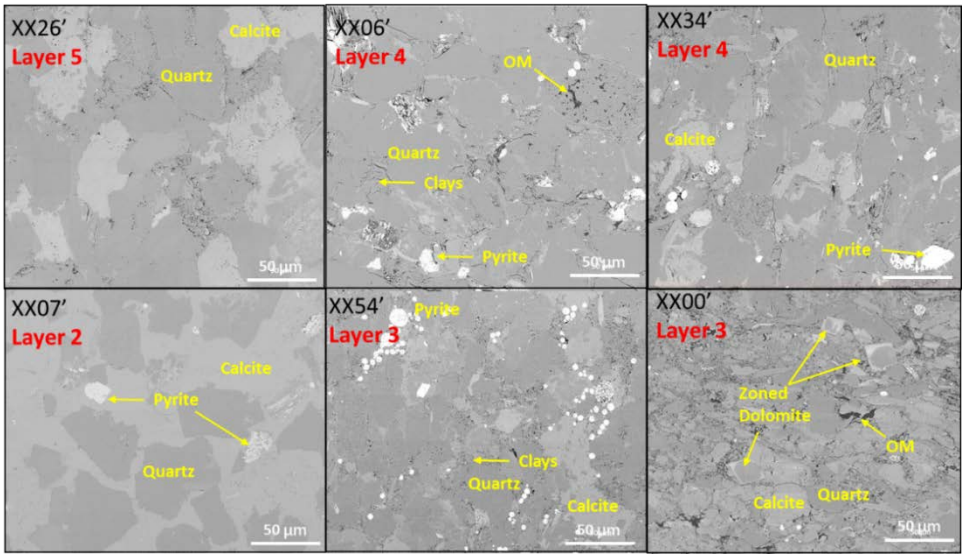

Figure 5.4 SEM images of samples from layer 2,3,4, and 5. All scale bars are same (50 µm). Significant variation in rock microstructure observed throughout the well. Variations in grain size as well as dominant mineralogy is observed. No strong preference for orientation of grains which matches with the low anisotropy calculated from velocity measurement.

5.3 Porosity

Porosity measurements in this study consist of a combination of helium porosity and NMR porosity measurement on dry samples. The helium resolves all the vacant pore space and the NMR captures the fluid remaining in the pore space. The sum of the two yields a total porosity. The total porosity of samples from different wells is shown in **Figure 5.5**. The order of the wells follows the depositional trend (NW-SE). It shows that wells have a similar porosity range, 0-9%, and the porosity range does not change with the deposition.

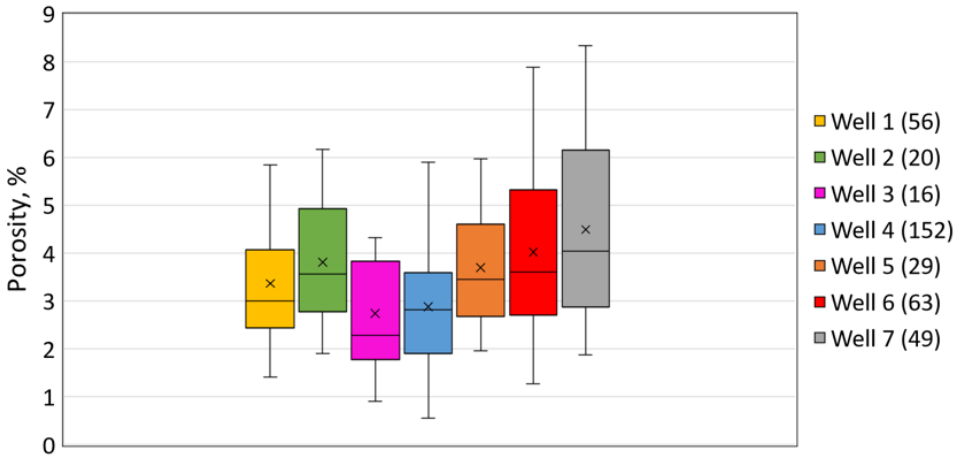

Figure 5.5 Total porosity of samples from different wells. The total number of samples from each well are shown in the brackets. The well order follows the depositional trend. Different wells are shown in different colors.

5.4 Mineralogy

Transmission Fourier Transform Infrared spectroscopy (FTIR) provides quantitative mineralogy. FTIR overcomes technical challenges in sample preparation or data acquisition (Harville and Freeman, 1988; Sondergeld and Rai, 1993; Herron et al. 1997; Ballard, 2007; Herron et al. 2014). It mainly depends on the detection of the vibrational energy of molecular bonds in order to quantify mineralogy. Studies have shown that 90% of the time, FTIR gives mineralogy quantification that is within +/-5 wt% of the actual mineralogy (Ruessink and Harville, 1992; Ballard, 2007). Mineralogy of each sample is measured using the transmission FTIR, shown in **Figure 5.6**. Wells are in the order of the depositional trend (NW-SE). Different

minerals are shown in different colors. Following the depositional trend, the clay content increases from NW to SE.

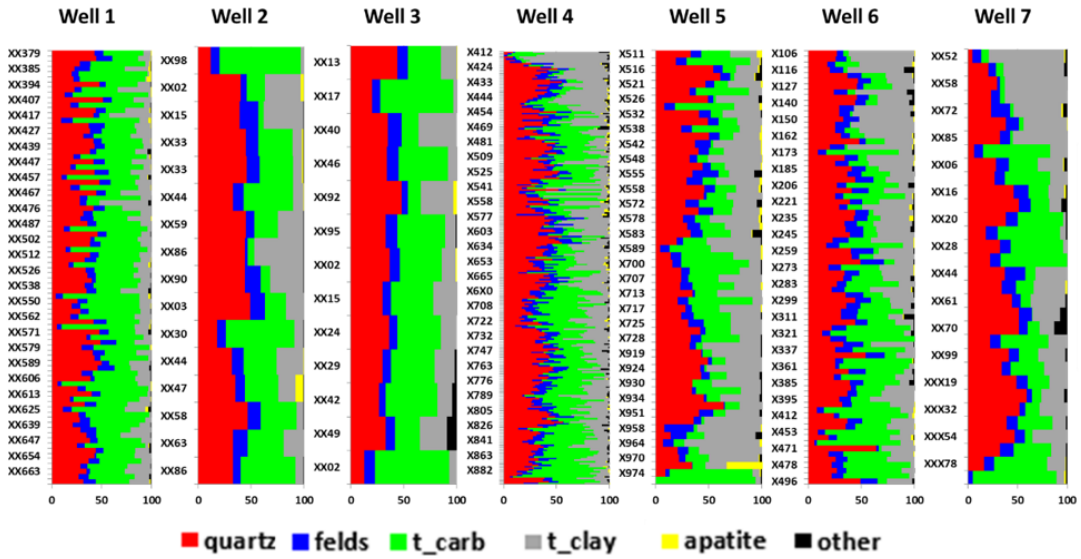

Figure 5.6 Mineralogy measured using transmission FTIR. Wells are in the order of depositional trend (NW-SE). Different minerals are shown in different colors. The higher frequency displayed in well 4 is simply a consequence of finer sampling.

FTIR provides the mineralogy limited to the access of plug samples. In order to acquire a high spatial resolution mineralogy profiles, the mineralogy inverted from XRF elemental data was used. **Figure 5.7** shows the comparison between FTIR mineralogy and XRF mineralogy (inverted from XRF elements using internal inversion software). The x-axis is XRF mineralogy, and the y-axis is FTIR mineralogy. Overall, XRF and FTIR mineralogy are in good agreement.

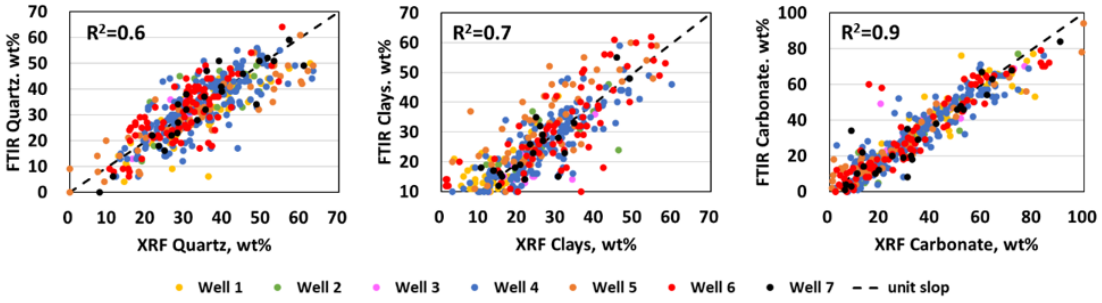

Figure 5.7 XRF-FTIR mineralogy comparison. The x-axis is FTIR mineralogy in weight percentage and the y-axis is XRF mineralogy inverted from XRF elements in weight percentage. They show a reasonable match.

Mineralogy measured using XRF is shown in **Figure 5.8**. Mineralogy is measured from X-ray fluorescence (XRF), which can provide a high spatial resolution, i.e.1-2 inch. From left to right, the wells are in the order of the depositional trend. Meramec formation is classified into zones 1 through 7, shown as solid lines. Following the depositional trend, the clay content increase from wells 1 to 7. From northwest to southeast in the distal direction, it is found that calcite concentration decreases, whereas clay concentration increases.

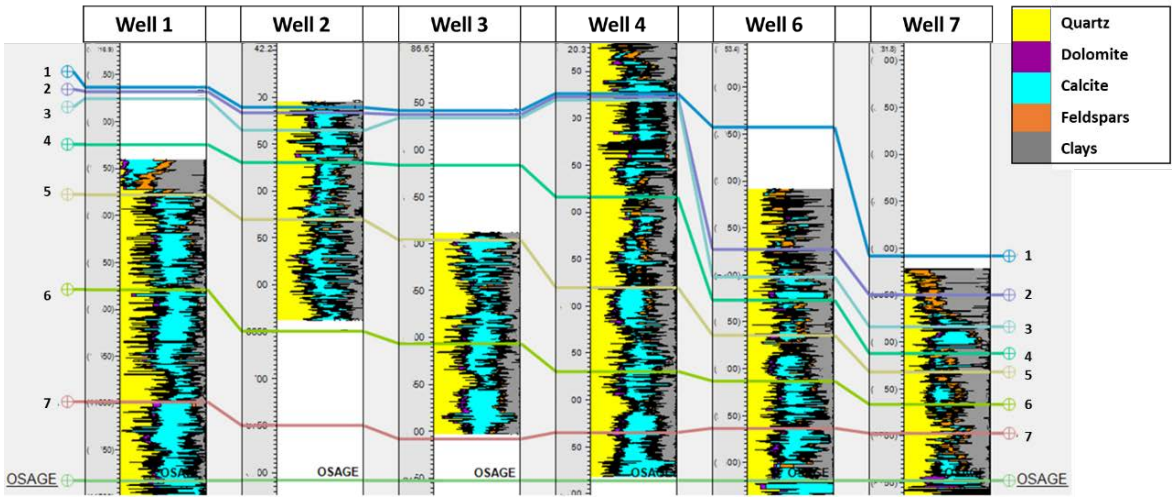

Figure 5.8 Mineralogy measured using XRF. Wells are in the order of the depositional trend (NW-SE). Different minerals and Meramec zonation are shown in different colors. Following the depositional trend, the clay content is increasing.

5.5 Velocity – porosity, mineralogy relationship

To investigate the effect of porosity and mineralogy on velocities, a scatterplot of velocities acquired at 4000psi, mineralogy, total porosity is shown in **Figure 5.9**. Clear trends indicate that both Vp and Vs decrease with increasing porosity and clay content. The following fits to the data are obtained by least-squares regression. For compressional velocity (velocities in km/sec, porosity is the volume fraction pores, Clays is the weight fraction clay),

$$Vp = 6.4 - 1.5*Clays - 15.5*\emptyset \ (R^2=0.5) \quad \text{Eq 5-3}$$

and for the shear velocity.

$$Vs = 3.6 - 0.9*Clays - 5.1*\emptyset \ (R^2=0.4) \quad \text{Eq 5-4}$$

The coefficients for porosity and clay content show that velocities are more sensitive to porosity than mineralogy.

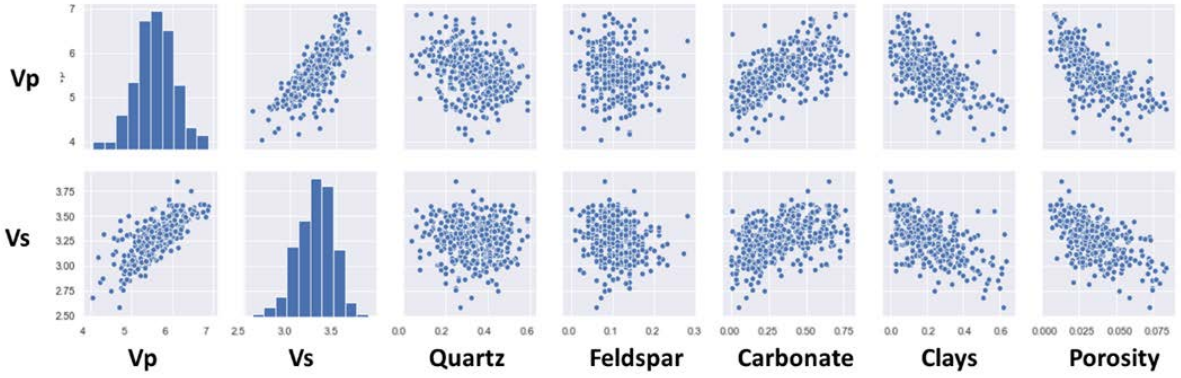

Figure 5.9 Scatter plots of porosity, mineralogy and velocity. Vp and Vs show a clear linear trend. Both Vp and Vs decrease with increasing porosity and clay content. There is no clear correlation between quartz, feldspar, and velocity.

5.6 Pressure dependence

Pressure strongly influences the mechanical and transport properties of rocks, such as acoustic velocity and porosity (Dobróka and Molnár, 2012). The velocity of acoustic waves propagating in different rocks under various confining pressure conditions (Wyllie et al. 1958; Stacey 1976; Prasad and Manghnani 1997; King 2009) have been investigated for several decades. The phenomenon that the wave velocity increases with pressure is well-known and has been explained in various rock mechanical studies (Wyllie et al. 1956; Birch 1960). One of the most frequently used explanations the phenomenon is based on the closure of microcracks in rocks under the change of pressure (Holt et al. 1997; Best 1997; Hassan and Vega 2009; Sengun et al. 2011). In cracked rocks, for instance, crack density and geometry influence elastic wave

velocity (Walsh, 1965) while crack fabric (preferential orientation) may result in the development of elastic anisotropy (Nishizawa, 1982).

The pressure dependence of velocities are shown in **Figure 5.10** and **Figure 5.11**. **Figure 5.10** shows all the horizontal samples that have low gamma, and **Figure 5.11** shows all vertical samples. The effective pressure range is from 500 psi to 4000 psi. From **Figure 5.10,** the Vs_slow is more sensitive to pressure change compare to Vs_fast. Therefore, most of the cracks are parallel to bedding planes. Both vertical and horizontal samples have small velocity difference (<10%) from low effective pressure to high effective pressure. The differences are small, i.e. less than 10%. Therefore, the velocity dependence on pressure is small.

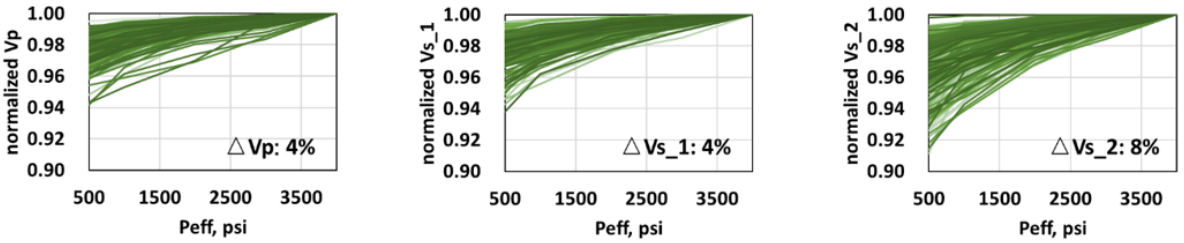

Figure 5.10 Acoustic velocities of all horizontal samples as a function of effective pressure. Effective pressure is from 500 psi to 4000 psi.

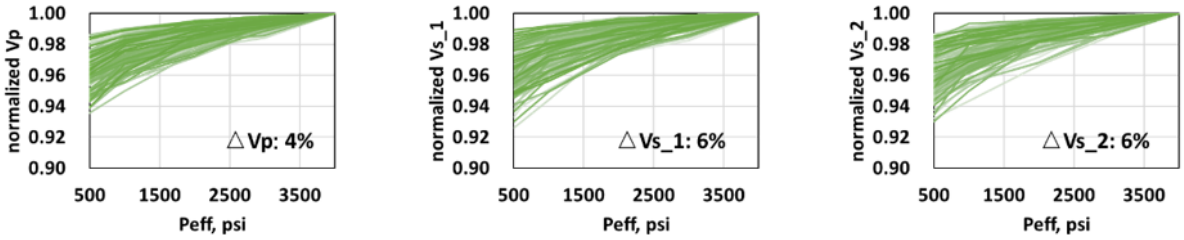

Figure 5.11 Acoustic velocities of all vertical samples as a function of effective pressure. Effective pressure is from 500 psi to 4000 psi.

5.7 Velocity systematics (Wells)

We propose two approaches to estimate Vs from Vp. These regressions can be applied to wireline Vp, which was measured in the vertical direction. In this section, all the velocity data are dodecane saturated velocities measured at 4000 psi.

5.7.1 Method 1

The first method is combining both Vp and Vs measured from all vertical plugs and low anisotropy horizontal plugs to create a single systematic. More than 90% of horizontal samples have low anisotropy (i.e. <=10%), shown in **Figure 5.12**. In other words, both vertical samples and low anisotropy horizontal samples were considered equivalent.

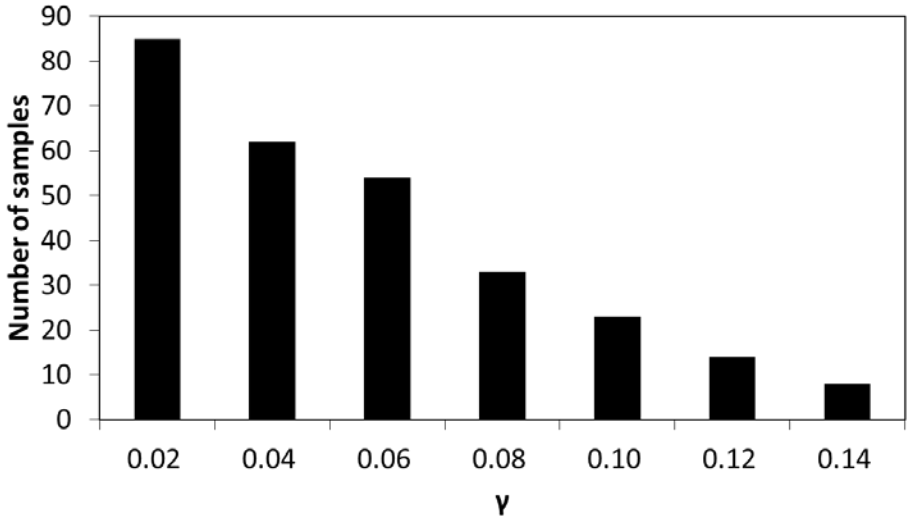

Figure 5.12 Shear wave anisotropy of all horizontal samples. More than 90% of samples have an anisotropy parameter, γ, of less than 0.1.

The measured Vp and Vs of vertical and horizontal samples with low γ are plotted in **Figure 5.13**. Wells are indicated by different colors. The average Vp and Vs follow a similar trend regardless of well location. Therefore, combining all well data, using weighted least squares (WLSQ) regression, a Vp-Vs systematic equation can be generated (Eq 5-5).

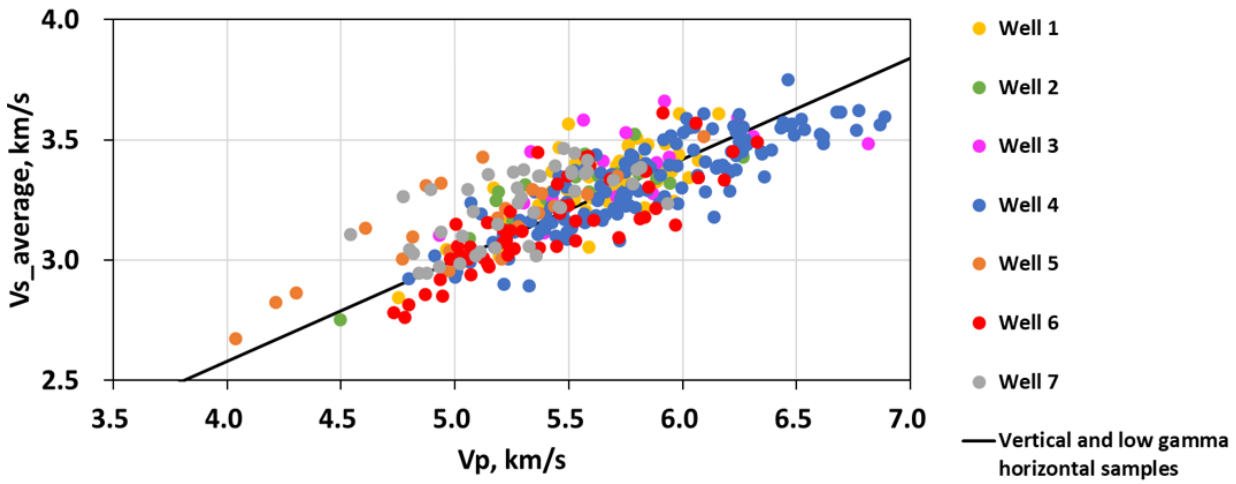

Figure 5.13 Measured velocities on all vertical and low γ horizontal samples from all wells. The measured velocities from different wells are shown in different colors. The correlation between Vp-Vs is shown as a black line.

$$Vs = 0.90 + 0.42*Vp \ (R^2=0.7) \qquad \text{Eq 5-5}$$

Where,

Vp is compressional wave velocity, km/sec

Vs is shear wave velocity, km/sec

5.7.2 Method 2

The second method uses Thomsen's anisotropy parameter ε to corrected Vp measured from horizontal plugs to make it equivalent to measured vertical Vp. Sondergeld and Rai (2011) observed there is a correlation between γ and ε, shown in **Figure 5.14**:

$$\gamma=1.41\varepsilon-0.054 \qquad \text{Eq 5-6}$$

Using the gamma-epsilon equation Eq 5-6 and Eq 5-2, Vp_horizontal can be converted to Vp_vertical.

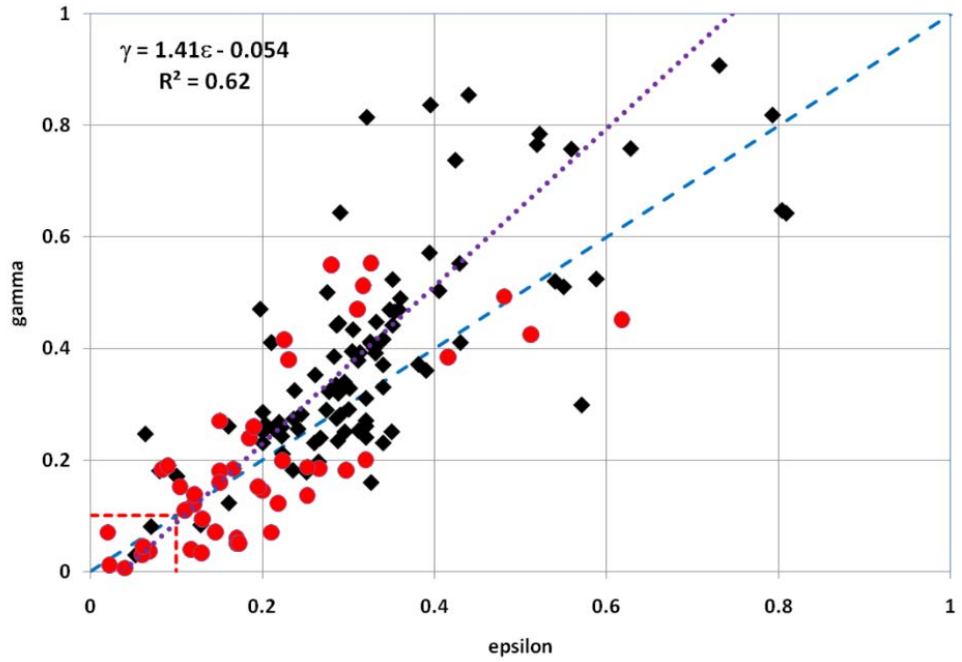

Figure 5.14 Correlation between gamma and epsilon (Sondergeld and Rai, 2011).

The vertical sample velocities and converted horizontal sample velocities are plotted in **Figure 5.15**. Wells are presented in different colors. Vp and Vs_slow follow a similar trend regardless of the well location. Combining all well data, using Weighted Least Squares (WLS) regression, a Vp-Vs systematic equation can be generated (Eq 5-7).

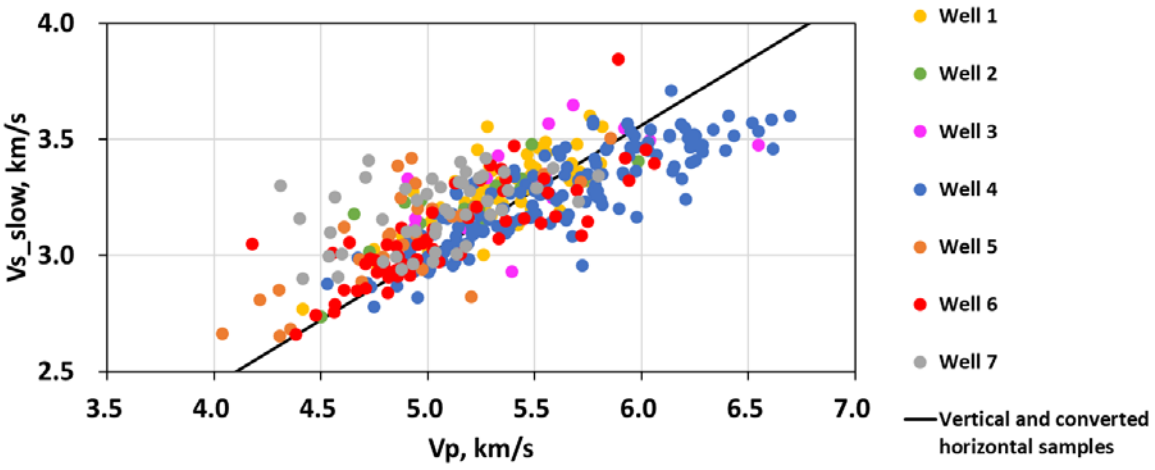

Figure 5.15 Measured vertical and converted horizontal sample velocities of all wells. The velocities of different wells are shown in different colors. The correlation of Vp-Vs is shown as a black line.

$Vs = 0.20 + 0.56*Vp$ ($R^2=0.6$) Eq 5-7

Where,

Vp is compressional wave velocity, km/sec

Vs is shear wave velocity, km/sec

Using Eq 5-5 and Eq 5-7, the Vs residuals (**Figure 5.16**) can be calculated. The range of Vs residuals using the first and second method is -0.4 to 0.4 and -0.6 to 0.6, respectively. The first method shows a narrower residual range. Therefore, the first method provides a better estimation than the second method. This might be due to the gamma-epsilon equation relations for samples having anisotropy parameters between 0 to 1. We recommend using Eq 5-5 to estimate Vs in Meramec formation.

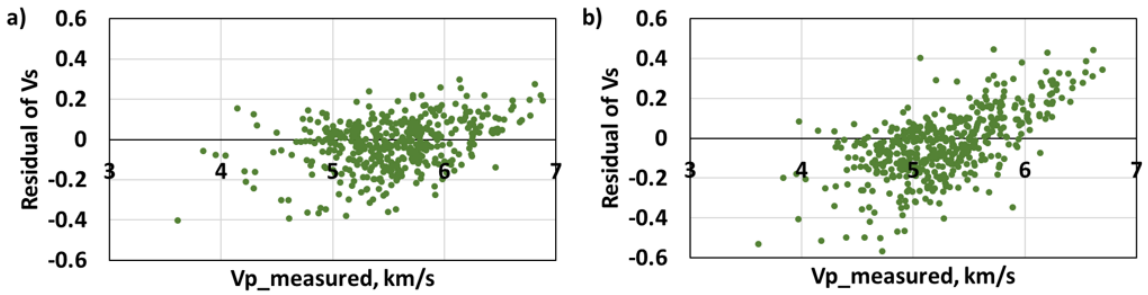

Figure 5.16 Vs residuals using the Vp-Vs equation. a) Vs residuals calculated using the equation created from the first method. The residuals range between -0.4 to 0.4; b) Vs residuals calculated using the equation created from the second method. The residual range between -0.6 to 0.6.

5.7.3 Validation

We tested our shear velocity systematic against well log data. Two wells that had sonic logs (compressional and shear velocities), gamma-ray log, and caliper log were selected. The well locations are shown in **Figure 5.17**, the first test well is 10 miles away from Well 4 and the

second test well is 10 miles away from Well 7. The comparisons between measure Vs and predicted Vs of the first and second test wells are shown in **Figure 5.18.** The Vp and Vs from the wireline are shown as grey and black lines, respectively. The predicted Vs using Meramec Vp-Vs systematic (Eq 5-5) is shown as the red line. There is a decent agreement between the measured Vs and predicted Vs in both test wells suggesting that the Meramec velocity systematic can provide a reasonable Vs prediction. However, the second test well shows a more significant error than the first test well.

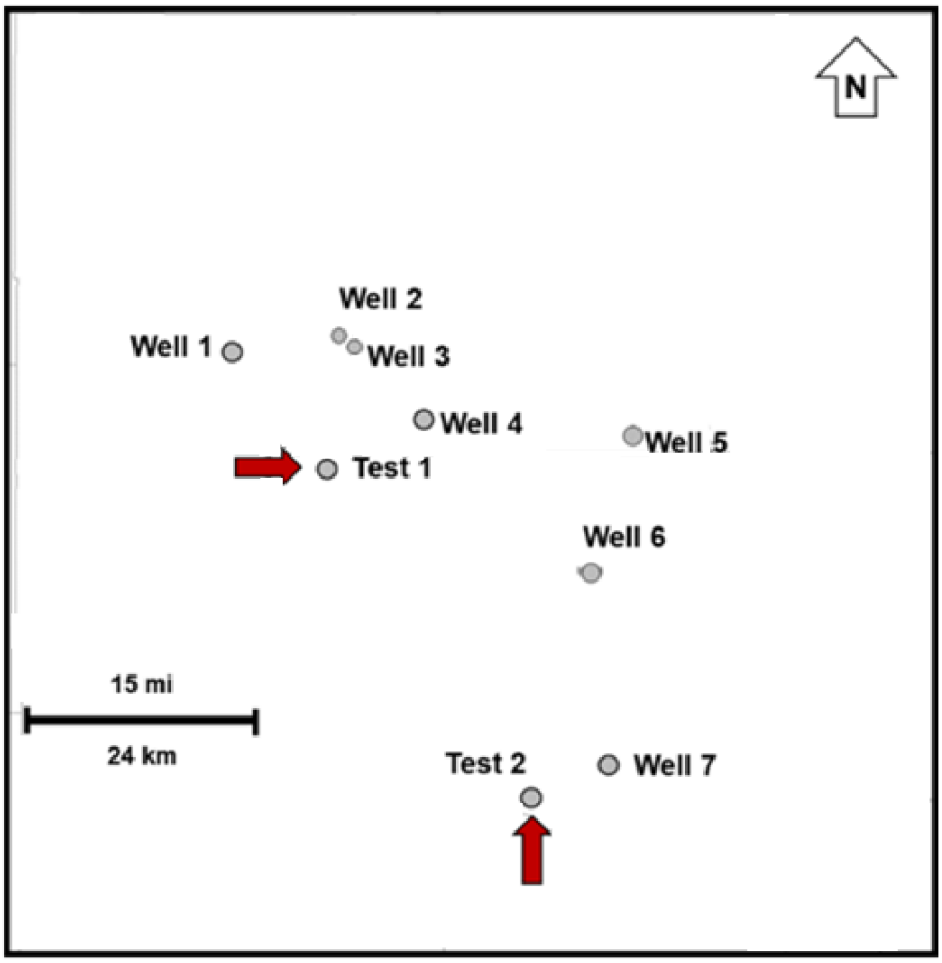

Figure 5.17 Test well locations are shown on the map. The first test well is 10 miles away from Well 4 and the second test well is 10 miles away from Well 7.

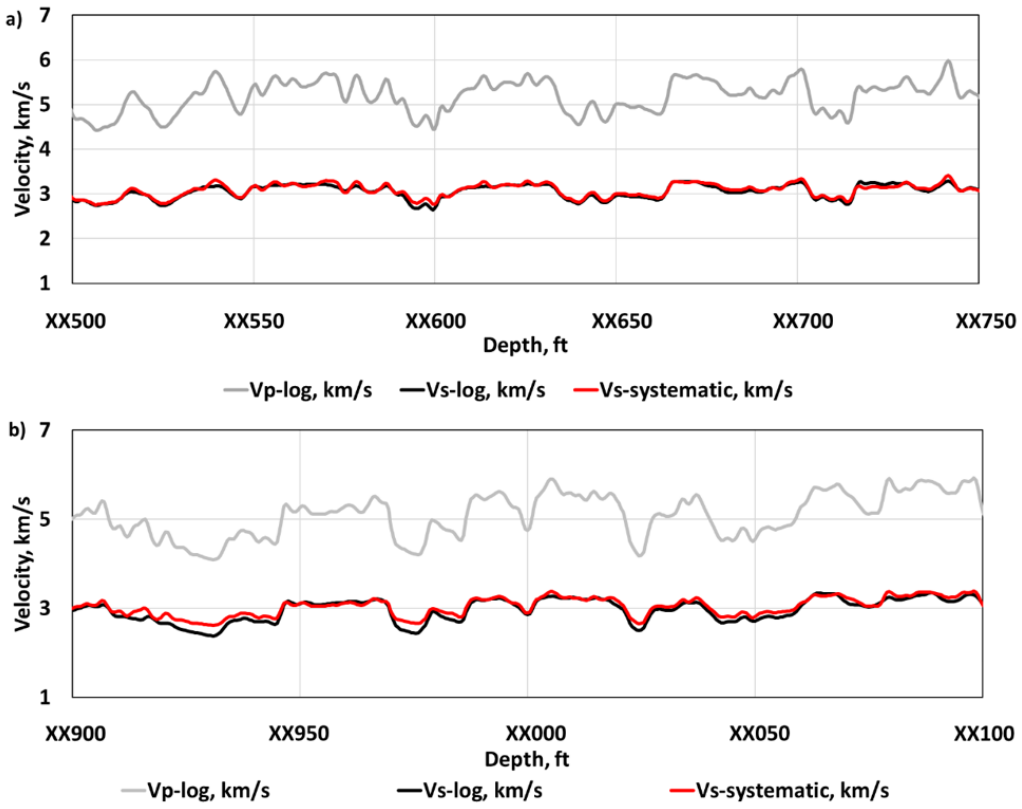

Figure 5.18 a) The Vp and Vs from wireline measurements, and predicted Vs using the Meramec velocity systematic(Eq 5-5) of first test well. b) The Vp and Vs from wireline measurement, and predicted Vs using the Meramec velocity systematic of first test well. The measured Vs and predicted Vs of both test wells show good agreement.

To investigate the reason of the estimation error, the composite log plots of the Vs residual (difference between Vs from sonic log and Vs predicted using systematic), gamma-ray log, Vsh, and caliper log are plotted, shown in **Figure 5.19** and **Figure 5.20.** Vsh is calculated from GR log using equation given by Larionov (1969):

$$V_{sh} = I_{GR} = \frac{GR_{log} - GR_{min}}{GR_{max} - GR_{min}} \quad \text{Eq 5-8}$$

$$V_{sh} = 0.0832(2^{3.7I_{GR}} - 1) \quad \text{Eq 5-9}$$

Where,

GR_{log}= the gamma ray reading at the depth of interest

GR_{min}= the minimum gamma ray reading.

GR_{max}= the maximum gamma ray reading.

IGR= gamma ray index

Vsh= Vsh= shale volume

It is evident that Vs estimation error is small in the test well 1. Noticed in the second test well, there are some washout zones, where borehole diameter is larger than the bit size, it caused a large Vs estimation error.

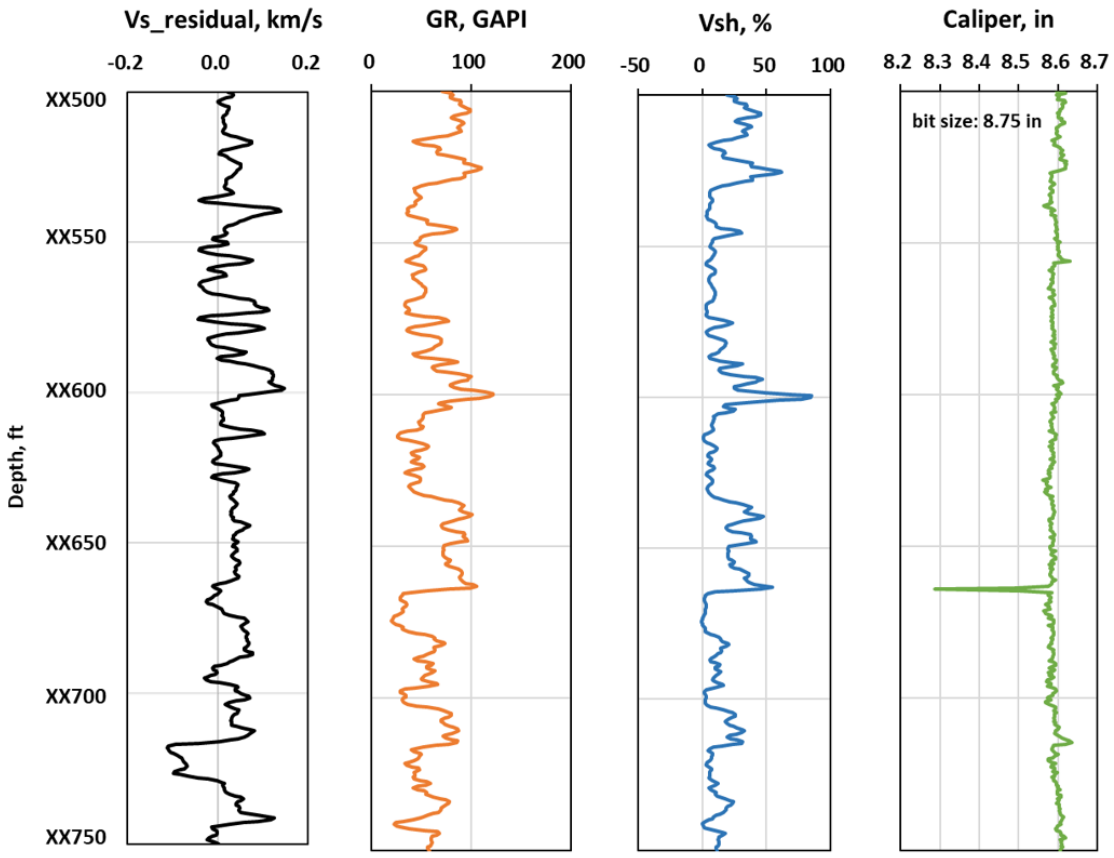

Figure 5.19 The Vs residual, GR log, Vsh estimated from GR log, and the caliper log for Test 1 well are shown as black, orange, blue and green, respectively. The velocity comparison between log and systematic is in the last track. The Vs estimation error is less than 6%.

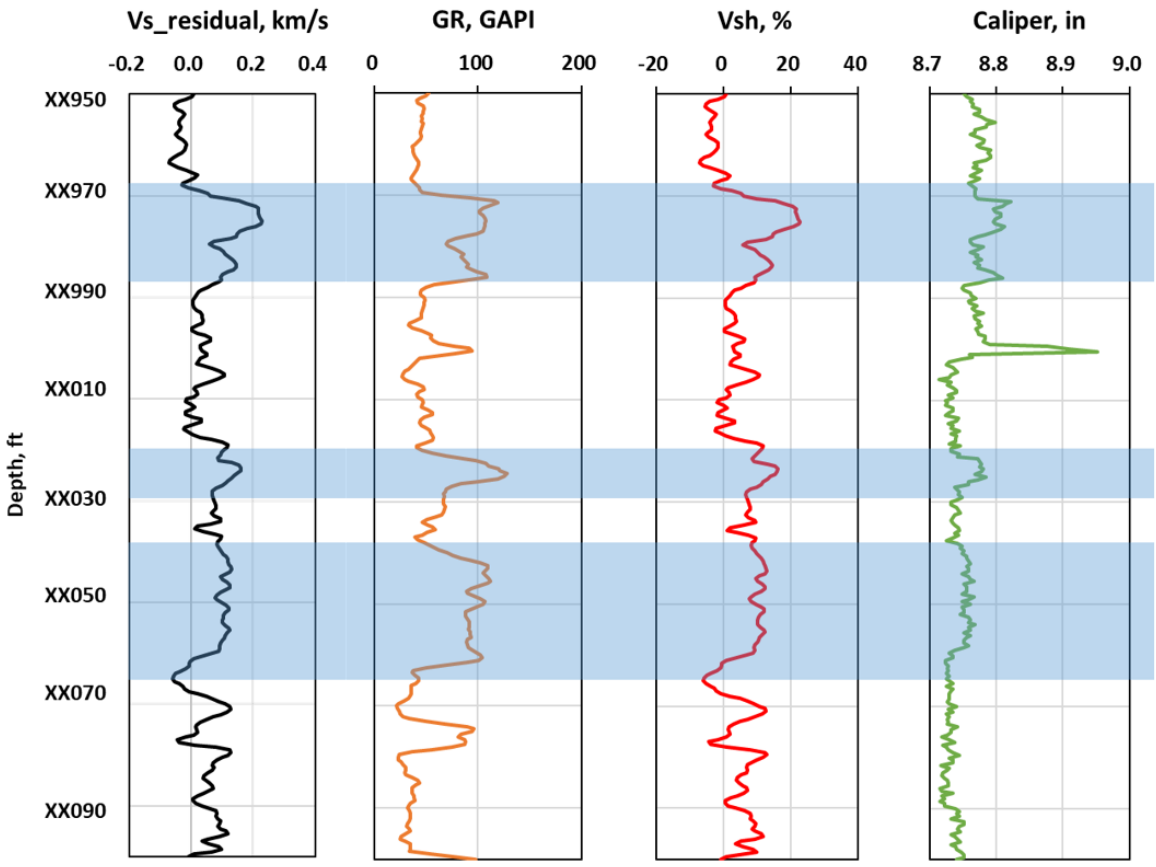

Figure 5.20 The Vs residual, GR log, Vsh estimated from GR log, and caliper log of test 2 well are shown as black, orange, blue and green, respectively. The velocity comparison between log and systematic is in the last track. Zones having large estimation errors are shown in the blue box. There is a positive correlation between washouts and Vs residual.

Figure 5.21 shows a combined shear-wave prediction reported in the literature and this study. It is evident that the Meramec Vp-Vs systematic has a unique trend compared to the Greenberg-Castagna trend line. Moreover, the Meramec velocity systematic also shows a unique trend compared to other unconventional systematics. This might due to the Meramec formation has little to no organics, as shown in **Figure 5.22**. Therefore, it is essential to create distinct shear wave prediction equations for different study areas.

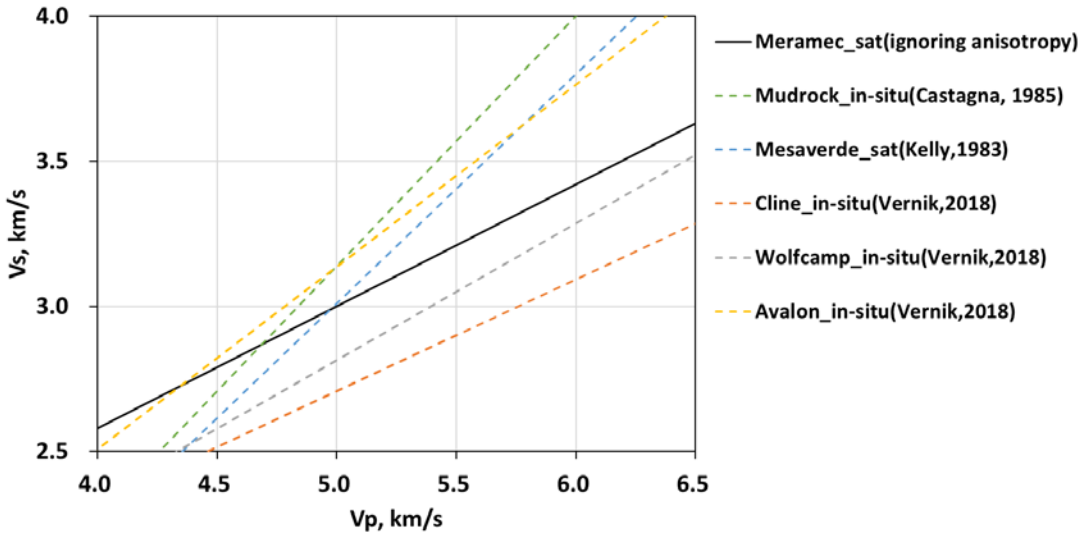

Figure 5.21 Comparison of Meramec formation systematic (WLSQ) with reported unconventional Vp-Vs velocity systematics (Vernik, 2018), including the Castagna mudrock systematic.

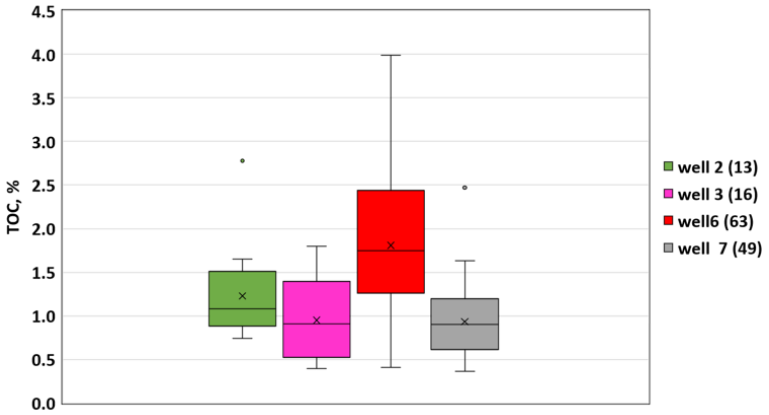

Figure 5.22 Leco™-TOC measured from wells 2, 3, 6, and 7. Number of samples are labeled following well names. It shows that the formation contains little to no organics (less than 5%).

5.8 Velocity systematics (Zonation)

To investigate if the Vp-Vs systematics changes with the depth, the Vp-Vs systematics of each Meramec layers was calculated. **Figure 5.23** shows the global onlap and sea-level curve for the Carboniferous-Permian period tied to a generalized Mississippian stratigraphic column and Meramec type log from the study area (Miller, 2019). The Meramec was deposited during a

transition from greenhouse to icehouse climate conditions, resulting in increasing cyclicity with the rise and fall of sea level, thus affecting deposition (Read, 1995). Price et al. (2017) also mentioned during Meramec deposition it shows increasing cyclicity. The gamma-ray response with the zonation of one of wells is shown as an example of zonation classification. It shows a similar trend with increasing cyclicity.

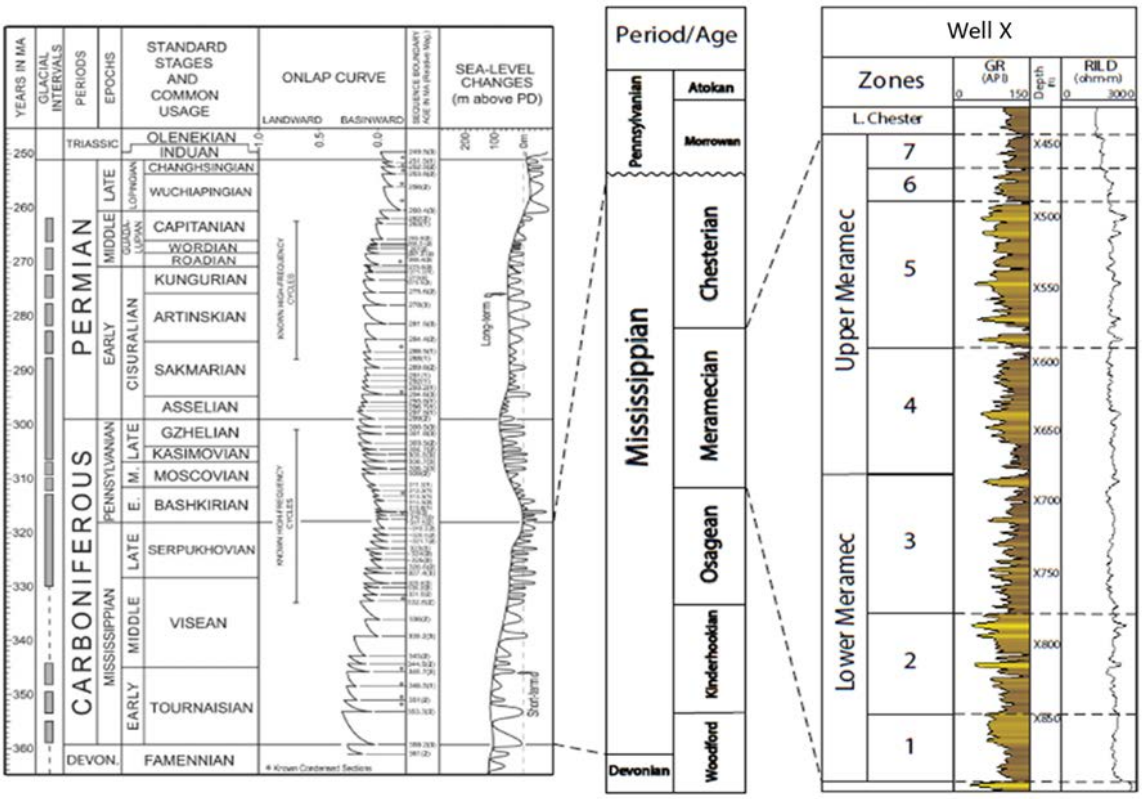

Figure 5.23. Mississippian stratigraphic column is displayed next to the sea level cyclicity of the Carboniferous and Permian periods. The Meramec is deposited during increasing cyclicity due in part to the climatic transition of the Mississippian, resulting in intricate stacking patterns and lateral distribution of facies. (Modified from Boyd, 2008; Haq and Schutter, 2008; Miller, 2019; Hardisty, 2019).

The analysis of Vp-Vs systematics for all wells shows the first method of ignoring anisotropy gives a better estimation than the second method considering anisotropy. Therefore, in this section, the Vp-Vs systematics of each Meramec layers was analyzed using the first method.

Both Vp and Vs measured from all vertical plugs and low anisotropy horizontal plugs are selected to create a single systematic. The measured Vp and Vs of vertical and horizontal samples with low γ are plotted for each Meramec zone, as shown in **Figure 5.24**. Zones 1 to 7 are indicated by different colors. The Vp and Vs show a linear correlation in all seven layers, however, with different pressure dependence slopes**.** A combination of Vp-Vs relation of seven layers is shown in **Table 5-2**. From **Table 5-2**, layers 1 to 3, layer 4, layers 5 to 7 have a small, large, and moderate slope, respectively. The layers are subsequently classified into three groups, as shown in **Figure 5.25**. The Vp-Vs relations of each group are shown in **Table 5-3**.

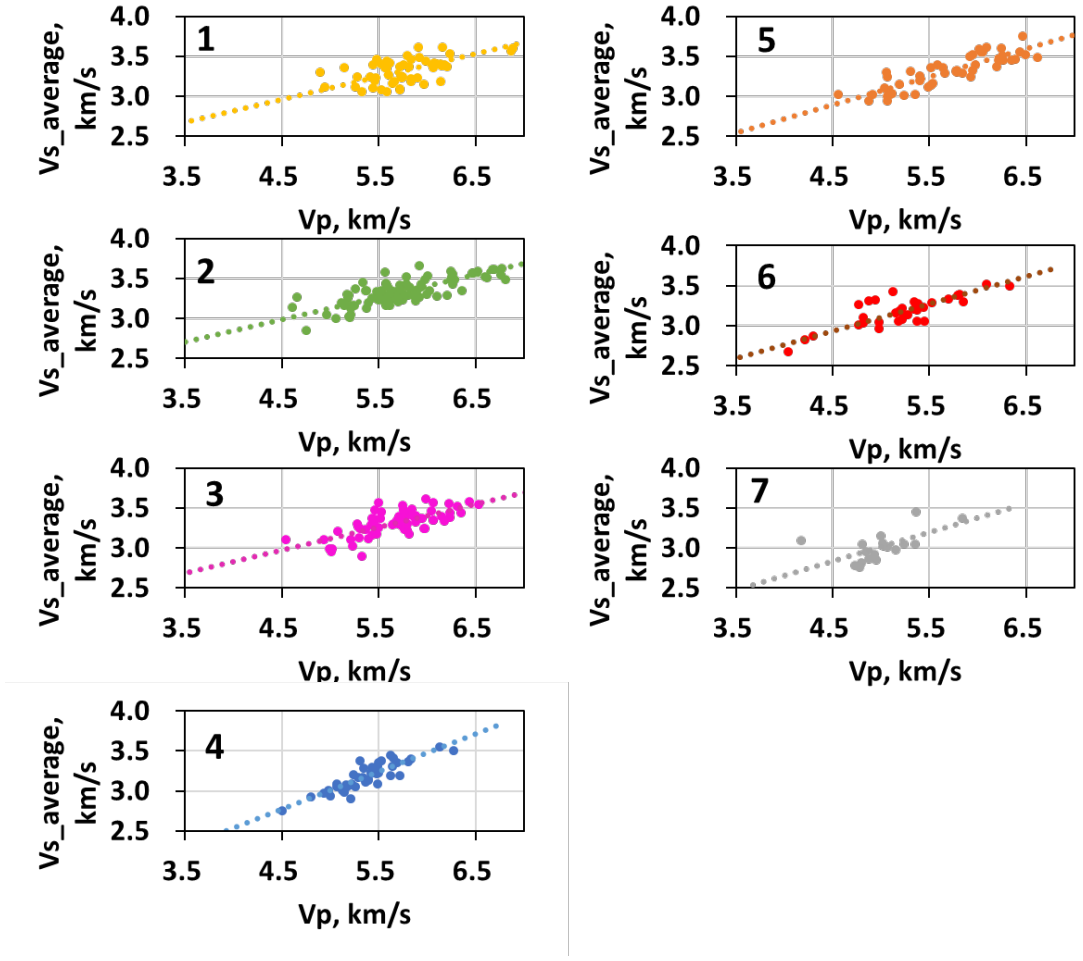

Figure 5.24 Measured vertical and low gamma horizontal sample velocities of Meramec zones. The velocities of different zones are shown in different colors. The correlations of Vp-Vs are shown as dash lines.

Table 5-2 Vp-Vs equations of all layers (velocities in km/sec)

$Vs = a_0 + a_1 * Vp$				
Zonation	a_0	a_1	R^2	Number of samples
1	1.68	0.28	0.3	55
2	1.72	0.28	0.6	99
3	1.68	0.29	0.5	74
4	0.66	0.47	0.8	46
5	1.30	0.35	0.7	52
6	1.41	0.34	0.6	37
7	1.21	0.36	0.3	22

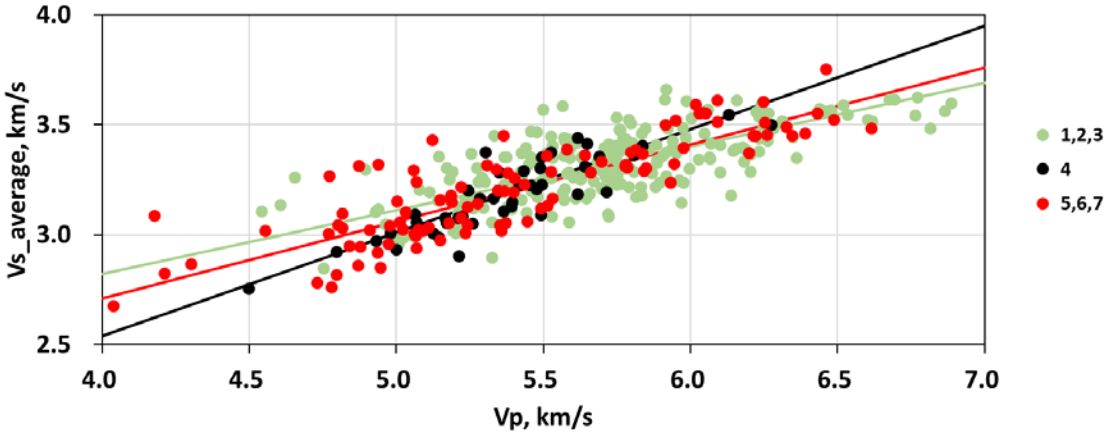

Figure 5.25 Measured vertical and low gamma horizontal sample velocities of grouped Meramec zones. The velocities of different groups are shown in different colors. The correlations of Vp-Vs are shown as solid lines.

The zonation classification also confirmed by the lithology, as shown in **Figure 5.26**. Miller (2019) classified Meramec lithology to mudstone, argillaceous siltstone, argillaceous calcareous siltstone, calcareous siltstone, and silty limestone from upper Meramec to lower Meramec. Zone 1-3, zone 4, and zone 5-7 have similar lithology, respectively. Therefore, the zonations can be classified into three groups and the Vp-Vs equations for each group are different.

Table 5-3 Vp-Vs equations of grouped Meramec layers (velocities in km/sec)

$Vs = a_0 + a_1 * Vp$			
Zonation	a_0	a_1	R^2
1,2,3	1.66	0.29	0.5
4	0.66	0.47	0.8
5,6,7	1.31	0.35	0.7

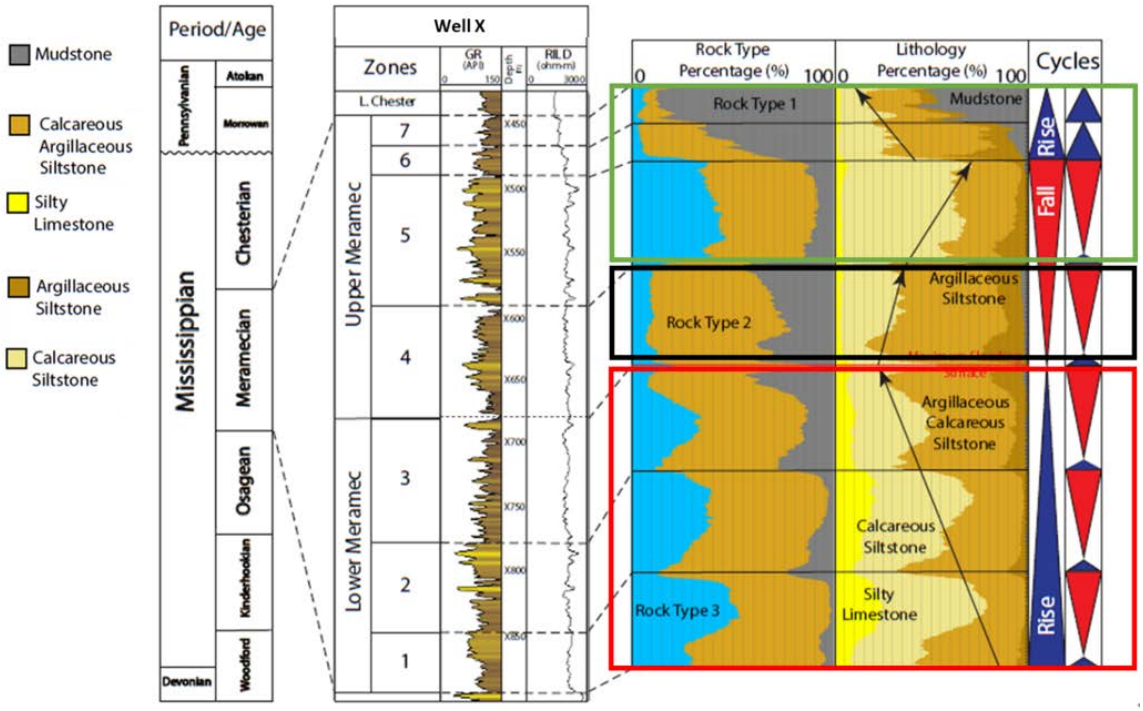

Figure 5.26 Generalized stratigraphic column of the Mississippian section on the left (Modified from Boyd, 2008) tied to a type log in the study area with interpreted internal zones of the Mississippian Meramec. The type log is tied to lithology and rock type vertical proportion curves on the right displaying the interpreted zones with the distribution of lithologies and rock types in the study area with interpreted 3rd and 4th order cycles (modified from Miller, 2019).

6 CONCLUSION

In this study, we have examined the shear wave velocity systematics of the Meramec formation. Several petrophysical properties, i.e. mineralogy and porosity, have been measured in order to investigate their effect on acoustic velocities. Based on our observations, we conclude the following:

1. Meramec samples have low velocity anisotropy, typically less than 10%.

2. The velocities are more sensitive to porosity than mineralogy. For compressional velocity ($\emptyset$ is the volume fraction pores, C is the weight fraction clay, and velocities are km/s),

$$V_p = 6.4 - 1.5C - 15.5\emptyset \ (R^2=0.5)$$

and for the shear velocity (km/s).

$$V_s = 3.6 - 0.9C - 5.1\emptyset \ (R^2=0.4)$$

3. Two approaches are proposed to estimate Vs from Vp; 1) ignoring anisotropy, i.e. analyzing velocity measurements from vertical plugs and low anisotropy horizontal plugs, we obtain:

$$V_s = 0.90 + 0.42V_p \ (R^2=0.7)$$

and 2) considering anisotropy, i.e. Vp measurements from horizontal plugs were corrected based on the Thomsen's compressional wave anisotropy parameter, we obtain:

$$V_s = 0.20 + 0.56V_p \ (R^2=0.6)$$

The first method shows a smaller Vs residual and is the preferred method. Estimated Vs by this method agrees well with the dipole wireline measurements.

When compared to the shear wave prediction equations reported in the literature, the Meramec Vp-Vs systematic show a distinct and different trend.

4. Meramec layers can be classified to three groups based on the slope of Vp-Vs equations and lithology:

Layers 1,2,3: $Vs = 1.66 + 0.29Vp$

Layer 4: $Vs = 0.66 + 0.47Vp$

Layers 5,6,7: $Vs = 1.31 + 0.35Vp$

7 REFERENCES

1. Ahmadov, R., 2011. Micro-textural, elastic and transport properties of source rocks: Ph.D. dissertation, Stanford University

2. Alkhalifah, T. and Rampton, D., 2001. Seismic anisotropy in Trinidad: A new tool for lithology prediction. The Leading Edge, 20(4), pp.420-424.

3. Aranibar, A., Saneifar, M. and Heidari, Z., 2013. Petrophysical rock typing in organic-rich source rocks using well logs. Unconventional Resources Technology Conference (URTEC). doi:10.1190/urtec2013-117

4. Asquith, G.B., Krygowski, D. and Gibson, C.R., 2004. *Basic well log analysis (Vol. 16).* Tulsa: American Association of Petroleum Geologists.

5. Baechle, G.T., Eberli, G.P., Weger, R.J. and Massaferro, J.L., 2009. Changes in dynamic shear moduli of carbonate rocks with fluid substitution. Geophysics, 74(3), pp. E135-E147.

6. Ball, M.M., Henry, M.E. and Frezon, S.E., 1991. Petroleum geology of the Anadarko Basin region, province (115), Kansas, Oklahoma, and Texas. US Geological Survey.

7. Ballard, B.D., 2007. Quantitative mineralogy of reservoir rocks using Fourier transform infrared spectroscopy. In SPE Annual Technical Conference and Exhibition. Society of Petroleum Engineers. doi:10.2118/113023-STU

8. Banik, N.C., 1984. Velocity anisotropy of shales and depth estimation in the North Sea basin. Geophysics, 49(9), pp.1411-1419.

9. Beebe, B.W., 1959. Characteristics of Mississippian production in the northwestern Anadarko basin: Tulsa Geological Society Digest, v. 27. *1959b, Characteristics of Mississippian production in the northwestern Anadarko basin*, pp.176-196.

10. Berryman, J.G., 1995. Mixture theories for rock properties. *Rock Physics and Phase Relations: A Handbook of physical constants*, 3, pp.205-228. Published under the aegis of the AGU Books Board.

11. Berryman, J.G., 2008. Exact seismic velocities for transversely isotropic media and extended Thomsen formulas for stronger anisotropies. Geophysics, 73(1), pp. D1-D10.

12. Best, A.I., 1997. The effect of pressure on ultrasonic velocity and attenuation in near‐surface sedimentary rocks. Geophysical Prospecting, 45(2), pp.345-364.

13. Birch, F., 1960. The velocity of compressional waves in rocks to 10 kilobars: 1. Journal of Geophysical Research, 65(4), pp.1083-1102.

14. Birch, F., 1961. The velocity of compressional waves in rocks to 10 kilobars: 2. Journal of Geophysical Research, 66(7), pp.2199-2224.

15. Boyd, D.T., 2008. *Stratigraphic guide to Oklahoma oil and gas reservoirs*: Oklahoma Geological Society. Special Publication, 1(2).

16. Brie, A., Pampuri, F., Marsala, A.F. and Meazza, O., 1995. Shear sonic interpretation in gas-bearing sands. In SPE Annual Technical Conference and Exhibition. Society of Petroleum Engineers. doi:10.2118/30595-MS

17. Broichhausen, H., Littke, R. and Hantschel, T., 2005. Mudstone compaction and its influence on overpressure generation, elucidated by a 3D case study in the North Sea. International Journal of Earth Sciences, 94(5-6), pp.956-978.

18. Castagna, J. P., Batzle, M. L. and Eastwood, R. L., 1985. Relationships between compressional-wave and shear-wave velocities in clastic silicate rocks. Geophysics, 50(4), pp.571-581. doi: 10.1190/1.1441933.

19. Castagna, J.P. and Backus, M.M. eds., 1993. *Offset-dependent reflectivity—Theory and practice of AVO analysis.* Society of Exploration Geophysicists.

20. Cheng, C.H. and Toksöz, M.N., 1979. Inversion of seismic velocities for the pore aspect ratio spectrum of a rock. Journal of Geophysical Research: Solid Earth, 84(B13), pp.7533-7543.

21. Crampin, S., 1984. An introduction to wave propagation in anisotropic media. Geophysical Journal International, 76(1), pp.17-28.

22. Daley, P.F. and Hron, F., 1977. Reflection and transmission coefficients for transversely isotropic media. Bulletin of the Seismological Society of America, 67(3), pp.661-675.

23. De Martini, D.C., Beard, D.C., Danburg, J.S. and Robinson, J.H., 1976. Variations of seismic velocities in sandstones and limestones with lithology and pore fluid at simulated in situ conditions. In Proc. EGPC Exploration Seminar (pp. 15-17).

24. DeVilbiss, J., Ito, H., and Nur, A., 1979. Measurement of compressional and shear wave velocities of water filled rocks during water-steam transition: Geophysics, 44, 407.

25. Digby, P.J., 1981. The effective elastic moduli of porous granular rocks.

26. Dobróka, M. and Molnár, J.S., 2012. New petrophysical model describing the pressure dependence of seismic velocity. Acta Geophysica, 60(2), pp.371-383.

27. Domenico, S.N., 1976. Effect of brine-gas mixture on velocity in an unconsolidated sand reservoir. Geophysics, 41(5), pp.882-894.

28. Drummond, K., 2018. Regional stratigraphy and proximal to distal variation of lithology and porosity within a mixed carbonate-siliciclastic system, Meramec and Osage series (Mississippian), central Oklahoma. Master's Thesis. University of Oklahoma.

29. Gassmann, F., 1964. Introduction to seismic travel time methods in anisotropic media. Pure and Applied Geophysics, 58(1), pp.63-112.

30. Gong, F., Di, B., Wei, J., Ding, P., Pan, X. and Zu, S., 2018. Ultrasonic velocity and mechanical anisotropy of synthetic shale with different types of clay minerals. Geophysics, 83(2), pp.MR57-MR66.

31. Greenberg, M. L., and J. P. Castagna, 1992. Shear-wave velocity estimation in porous rocks: Theoretical formulation, preliminary verification and applications: Geophysical Prospecting, 40, 195–209, doi: 10.1111/j .1365-2478.1992.tb00371.x.

32. Gretener, P. E., 1981. Geothermics--using temperature in hydrocarbon exploration: Education Course Notes Series No. 17, Am. Assn. Petr. Geol.

33. Gutschick, R.C. and Sandberg, C.A., 1983. Mississippian continental margins on the conterminous United States, in D. J. Stanley and G. T. Moore, The shelf break: Critical interface on continental margins: SEPM Special Publication 33, p. 79 – 96.

34. Han, D.H., Nur, A. and Morgan, D., 1986. Effects of porosity and clay content on wave velocities in sandstones. Geophysics, 51(11), pp.2093-2107.

35. Han, D.H., Nur, A. and Morgan, D., 1986. Effects of porosity and clay content on wave velocities in sandstones. Geophysics, 51(11), pp.2093-2107.

36. Han, H., Dang, S., Acosta, J.C., Fu, J., Sondergeld, C. and Rai, C., 2019. X-Ray Fluorescence and Laser Induced Breakdown Spectroscopy for Advanced Rock Elemental Analysis. Unconventional Resources Technology Conference (URTEC). doi:10.15530/urtec-2019-1072

37. Haq, B.U. and Schutter, S.R., 2008. A chronology of Paleozoic sea-level changes. Science, 322(5898), pp.64-68.

38. Hardisty, L., 2019. Stratigraphic Variability of Mississippian Meramec Chemofacies and Petrophysical Properties Using Machine Learning and Geostatistical Modeling, STACK Trend, Anadarko Basin, MS thesis, The University of Oklahoma.

39. Hardwick, J., 2018. Reservoir Quality Evaluation of the Meramec and Upper Osage Units in the Anadarko Basin. Master's Thesis. University of Oklahoma.

40. Harville, D. G. and Freeman, D.L., 1988. The benefits and application of rapid mineral analysis provided by Fourier Transform Infrared Mineralogy, SPE 18120, 141-150. doi:10.2118/18120-MS

41. Hassan, A. and Vega, S., 2009. June. A study of seismic velocities and differential pressure dependence in a Middle East carbonate reservoir. In 71st EAGE Conference and

Exhibition-Workshops and Fieldtrips (pp. cp-129). European Association of Geoscientists & Engineers.

42. Herron, M.M., Matteson, A. and Gustavson, G., 1997. Dual-range FT-IR mineralogy and the analysis of sedimentary formations. Proceeding of the 1997 Society of Core Analysts, 7-10 September, Calgary, Paper SCA-9729.

43. Herron, S., Herron, M., Pirie, I., Saldungaray, P., Craddock, P., Charsky, A., Polyakov, M., Shray, F. and Li, T., 2014. Application and quality control of core data for the development and validation of elemental spectroscopy log interpretation. Petrophysics, 55(05), pp.392-414.

44. Hickman, G., 2018. Parasequence-Scale Stratigraphic Variability of Lithology and Porosity of Mississippian Meramec Reservoirs and the Relationships to Production Characteristics, STACK Trend, Oklahoma. Master's Thesis. University of Oklahoma.

45. Holt, R.M., Furre, A.K. and Horsrud, P., 1997. Stress dependent wave velocities in sedimentary rock cores: Why and why not? International Journal of Rock Mechanics and Mining Sciences, 34(3-4), pp.128-e1.

46. Hornby, B.E., Schwartz, L.M. and Hudson, J.A., 1994. Anisotropic effective-medium modeling of the elastic properties of shales. Geophysics, 59(10), pp.1570-1583.

47. Jennings Jr, J.W. and Lucia, F.J., 2001. Predicting permeability from well logs in carbonates with a link to geology for interwell permeability mapping. In SPE Annual Technical Conference and Exhibition. Society of Petroleum Engineers.

48. Johnston, J.E. and Christensen, N.I., 1995. Seismic anisotropy of shales. Journal of Geophysical Research: Solid Earth, 100(B4), pp.5991-6003.

49. Jones, L.E. and Wang, H.F., 1981. Ultrasonic velocities in Cretaceous shales from the Williston basin. Geophysics, 46(3), pp.288-297.

50. Kern, H., Popp, T., Gorbatsevich, F., Zharikov, A., Lobanov, K.V. and Smirnov, Y.P., 2001. Pressure and temperature dependence of VP and VS in rocks from the superdeep well and from surface analogues at Kola and the nature of velocity anisotropy. Tectonophysics, 338(2), pp.113-134.

51. King, M.S., 2009. Recent developments in seismic rock physics. International Journal of Rock Mechanics and Mining Sciences, 46(8), pp.1341-1348.

52. Kirchberger, L.A., 2001. Investigation of elastic parameters at chosen well locations in the Vienna Basin. Diploma thesis, Montanuniversita¨t Leoben, Austria. Unpublished.

53. Kowallis, B.J., Jones, L.E.A. and Wang, H.F., 1984. Velocity - porosity - clay content systematics of poorly consolidated sandstones. Journal of Geophysical Research: Solid Earth, 89(B12), pp.10355-10364.

54. Kuster, G.T. and Toksöz, M.N., 1974. Velocity and attenuation of seismic waves in two-phase media: Part I. Theoretical formulations. Geophysics, 39(5), pp.587-606.

55. Lane, H.R. and De Keyser, T.L., 1980. Paleogeography of the late Early Mississippian (Tournaisian 3) in the central and southwestern United States. In: Paleozoic Paleogeography of West-Central United States Rocky Mountain paleogeography

symposium 1 (Eds T.D. Fouch and E.R. Magathan), SEPM, Rocky Mtn. Section, pp. 149–159.

56. Larionov, V.V., 1969. Borehole radiometry. Nedra, Moscow, 127.

57. Lo, T.W., Coyner, K.B. and Toksoz, M.N., 1986. Experimental determination of elastic anisotropy of Berea sandstone, Chicopee shale, and Chelmsford granite. Geophysics, 51(1), pp.164-171.

58. Lucia, F.J., 2007. *Carbonate reservoir characterization: An integrated approach*. Springer Science & Business Media.

59. Lucier, A.M., Hofmann, R. and Bryndzia, L.T., 2011. Evaluation of variable gas saturation on acoustic log data from the Haynesville Shale gas play, NW Louisiana, USA. The Leading Edge, 30(3), pp.300-311.

60. Marion, D. and Jizba, D., 1992. Acoustic properties and their dependence on porosity, mineralogy and saturation: applications to field-scale measurements. In Third European Core Analysis Symposium Soc. of Core AnalParis.

61. Mattaboni, P. and Schreiber, E., 1967. Method of pulse transmission measurements for determining sound velocities. Journal of Geophysical Research, 72(20), pp.5160-5163.

62. Mavko, G., Mukerji, T. and Dvorkin, J., 2020. The Rock Physics Handbook. Cambridge university press.

63. Mavko, G.M. and Nur, A., 1978. The effect of nonelliptical cracks on the compressibility of rocks. Journal of Geophysical Research: Solid Earth, 83(B9), pp.4459-4468.

64. Miller, M., 2019. Mississippian Meramec lithologies and petrophysical property variability, STACK trend, Anadarko Basin, Oklahoma, M.S. Thesis, University of Oklahoma, Norman, Oklahoma, 60 p.

65. Murphy III, W.F., Winkler, K.W. and Kleinberg, R.L., 1984. Frame modulus reduction in sedimentary rocks: The effect of adsorption on grain contacts. Geophysical Research Letters, 11(9), pp.805-808.

66. Murphy III, W.F., Winkler, K.W. and Kleinberg, R.L., 1986. Acoustic relaxation in sedimentary rocks: Dependence on grain contacts and fluid saturation. Geophysics, 51(3), pp.757-766.

67. NDT Resource Center, 2017. Wave Propagation, https://www.nde-ed.org/EducationResources/CommunityCollege/Ultrasonics/Physics/wavepropagation.htm (accessed April 24, 2018)

68. Nishizawa, O., 1982. Seismic velocity anisotropy in a medium containing oriented cracks. Journal of Physics of the Earth, 30(4), pp.331-347.

69. Northcutt, R.A. and Campbell, J.A., 1996. Geological provinces of Oklahoma, Oklahoma Geol. Surv. Open File Rep., OF5–95.

70. Northcutt, R.A., Johnson, K.S. and Hinshaw, G.C., 2001. Geology and petroleum reservoirs in Silurian, Devonian, and Mississippian rocks in Oklahoma. In Silurian, Devonian, and Mississippian geology and petroleum in the southern mid-continent: 1999 Symposium Oklahoma Geological Survey Circular (Vol. 105, pp. 1-29).

71. Nur, A. and Simmons, G., 1969. Stress - induced velocity anisotropy in rock: An experimental study. Journal of Geophysical Research, 74(27), pp.6667-6674.

72. O'Connell, R.J. and Budiansky, B., 1974. Seismic velocities in dry and saturated cracked solids. Journal of Geophysical Research, 79(35), pp.5412-5426.

73. Omovie, S. and Castagna, J., 2017. Acoustic response to fluid properties in hydrocarbon-rich shales. In 2017 SEG International Exposition and Annual Meeting. Society of Exploration Geophysicists.

74. Omovie, S.J. and Castagna, J.P., 2019. P-to-S-wave velocity ratio in organic shales. Geophysics, 84(6), pp.MR205-MR222.

75. Perry, W.J., 1989. Tectonic evolution of the Anadarko Basin region, Oklahoma (No. 1866). Department of the Interior, US Geological Survey.

76. Pickett, G.R., 1963. Acoustic character logs and their applications in formation evaluation. Journal of Petroleum technology, 15(06), pp.659-667.

77. Prasad, M. and Manghnani, M.H., 1997. Effects of pore and differential pressure on compressional wave velocity and quality factor in Berea and Michigan sandstones: Geophysics.

78. Price, B., K. Haustveit, and Lamb,A., 2017. Influence of stratigraphy on barriers to fracture growth and completion optimization in the Meramec Stack Play, Anadarko Basin, Oklahoma: Unconventional Resources Technology Conference (URTEC). doi:10.15530/URTEC-2017-2697585

79. Price, B.J., Pollack, A.C., Lamb, A.P., Peryam, T.C. and Anderson, J.R., 2020. Depositional interpretation and sequence stratigraphic control on reservoir quality and distribution in the Meramecian Sooner trend Anadarko Basin, Canadian, and Kingfisher Counties (STACK) play, Anadarko Basin, Oklahoma, United States. AAPG Bulletin, 104(2), pp.357-386.

80. Quirein, J., Far, M., Gu, M., Gokaraju, D. and Witkowsky, J., 2015. August. Relationships between sonic compressional and shear logs in unconventional formations. In SPWLA 56th annual logging symposium. Society of Petrophysicists and Well-Log Analysts.

81. Rai, C.S. and Hanson, K.E., 1988. Shear-wave velocity anisotropy in sedimentary rocks: A laboratory study. Geophysics, 53(6), pp.800-806.

82. Raymer, L.L., Hunt, E.R. and Gardner, J.S., 1980. An improved sonic transit time-to-porosity transform. In SPWLA 21st annual logging symposium. Society of Petrophysicists and Well-Log Analysts.

83. Read, J.F., 1995. Overview of carbonate platform sequences, cycle stratigraphy and reservoirs in greenhouse and icehouse worlds, in J.F. Read, C. Kerans, L.J. Weber, J. F. Sarg, and F.M. Wright, eds., Milankovitch sea level changes, cycles, and reservoirs on carbonate platforms in greenhouse and ice-house worlds: SEPM Short Course 35, p. 1-102.

84. Rickman, R., Mullen, M.J., Petre, J.E., Grieser, W.V. and Kundert, D., 2008. A practical use of shale petrophysics for stimulation design optimization: All shale plays are not clones of the Barnett Shale. In SPE annual technical conference and exhibition. Society of Petroleum Engineers. doi:10.2118/115258-MS

85. Ruessink, B.H. and Harville, D.G., 1992. Quantitative analysis of bulk mineralogy: The applicability and performance of XRD and FTIR. In SPE Formation Damage Control Symposium. Society of Petroleum Engineers. doi:10.2118/23828-MS

86. Saxena, V., Krief, M. and Adam, L., 2018. Handbook of Borehole Acoustics and Rock Physics for Reservoir Characterization. Elsevier.

87. Sayers, C.M., 2005. Seismic anisotropy of shales. Geophysical Prospecting, 53(5), pp.667-676.

88. Sengun, N., Altindag, R., Demirdag, S. and Yavuz, H., 2011. P-wave velocity and Schmidt rebound hardness value of rocks under uniaxial compressional loading. International Journal of Rock Mechanics and Mining Sciences (1997), 48(4), pp.693-696.

89. Simmons, G. and Brace, W.F., 1965. Comparison of static and dynamic measurements of compressibility of rocks. Journal of Geophysical Research, 70(22), pp.5649-5656.

90. Sondergeld, C.H. and Rai, C.S., 2011. Elastic anisotropy of shales. The Leading Edge, 30(3), pp.324-331.

91. Sondergeld, C.H. and Rai, C.S., 1993. A new concept in quantitative core characterization. The Leading Edge, 12(7), pp.774-779.

92. Sondergeld, C.H., Rai, C.S. and Whidden, R.W., 2000. Ultrasonic measurement of anisotropy on the Kimmeridge shale. In 2000 SEG Annual Meeting. Society of Exploration Geophysicists.

93. Stacy, T.R. and TR, S., 1976. Seismic assessment of rock masses. In: Bieniawski, Z.T. (ed.), Exploration for rock engineering, 2, Johannesburg, 113-118.

94. Teanby, N.A., Kendall, J.M. and Van der Baan, M., 2004. Automation of shear-wave splitting measurements using cluster analysis. Bulletin of the Seismological Society of America, 94(2), pp.453-463.

95. Thomsen, L., 1986. Weak elastic anisotropy. Geophysics, 51(10), pp.1954-1966.

96. Timur, A., 1977. Temperature dependence of compressional and shear wave velocities in rocks: Geophysics, 42, 950- 956.

97. Tosaya, C. and Nur, A., 1982. Effects of diagenesis and clays on compressional velocities in rocks. Geophysical Research Letters, 9(1), pp.5-8.

98. Tran, M.T., 2014. Formation evaluation of an unconventional shale reservoir: Application to the North Slope Alaska, PhD dissertation, Stanford University

99. Vanorio, T., Mukerji, T. and Mavko, G., 2008. Emerging methodologies to characterize the rock physics properties of organic-rich shales. The Leading Edge, 27(6), pp.780-787.

100. Vernik, L. and Liu, X., 1997. Velocity anisotropy in shales: A petrophysical study. Geophysics, 62(2), pp.521-532.

101. Vernik, L. and Milovac, J., 2011. Rock physics of organic shales. The Leading Edge, 30(3), pp.318-323.

102. Vernik, L. and Nur, A., 1992. Ultrasonic velocity and anisotropy of hydrocarbon source rocks. Geophysics, 57(5), pp.727-735.

103. Vernik, L., 1994. Predicting lithology and transport properties from acoustic velocities based on petrophysical classification of siliciclastics. Geophysics, 59(3), pp.420-427.

104. Vernik, L., 2016. Seismic petrophysics in quantitative interpretation. SEG Books.

105. Vernik, L., Castagna, J. and Omovie, S.J., 2018. S-wave velocity prediction in unconventional shale reservoirs. Geophysics, 83(1), pp.MR35-MR45.

106. Vernik, L., Fisher, D. and Bahret, S., 2002. Estimation of net-to-gross from P and S impedance in deepwater turbidites. The Leading Edge, 21(4), pp.380-387.

107. Walsh, J.B., 1965. The effect of cracks on the compressibility of rock. Journal of Geophysical Research, 70(2), pp.381-389.

108. Wang, Z., 2002. Seismic anisotropy in sedimentary rocks, part 1: A single-plug laboratory method. Geophysics, 67(5), pp.1415-1422.

109. Watt, J.P., Davies, G.F. and O'Connell, R.J., 1976. The elastic properties of composite materials. Reviews of Geophysics, 14(4), pp.541-563.

110. White, J.E., 1982. Computed waveforms in transversely isotropic media. Geophysics, 47(5), pp.771-783.

111. Wyllie, M.R.J., Gregory, A.R. and Gardner, G.H.F., 1958. An experimental investigation of factors affecting elastic wave velocities in porous media. Geophysics, 23(3), pp.459-493.